

Systematically Asymmetric: A comparison of H I profile asymmetries in real and simulated galaxies.

N. Deg,^{1,2*} S.-L. Blyth², N. Hank², S. Kruger², C. Carignan^{2,3}

¹*Department of Physics, Engineering Physics, and Astronomy, Queen's University, Kingston, ON, K7L 3N6, Canada*

²*Department of Astronomy, University of Cape Town, Private Bag X3, Rondebosch 7701, South Africa*

³*Observatoire d'Astrophysique de l'Université de Ouagadougou (ODAUO), BP 7021, Ouagadougou 03, Burkina Faso*

Accepted XXX. Received YYY; in original form ZZZ

ABSTRACT

We examine different measures of asymmetry for galaxy HI velocity profiles. We introduce the channel-by-channel asymmetry and the velocity-of-equality statistics to quantify profile asymmetries. Using a sample of simulated galaxies, we examine how these and the standard lopsidedness morphometric statistic depend on a variety of observational effects including the viewing angle and inclination. We find that our newly introduced channel-by-channel asymmetry is less sensitive to the effects of viewing angle and inclination than other morphometrics. Applying our statistics to the WHISP HI galaxy sample, we also find that the channel-by-channel asymmetry, is a better indicator of visually-classified asymmetric profiles. In addition, we find that the lopsidedness-velocity of equality space can be used to identify profiles with deep central dips without visual inspection.

Key words: radio lines: galaxies – galaxies: interactions – galaxies: evolution.

1 INTRODUCTION

Galaxies often appear axisymmetric on large scales, but a closer examination usually reveals a variety of asymmetric features. These include tidal tails, various stripping effects, off-centered spiral arms, and lopsidedness. At the smallest scales, even star formation can appear asymmetric. These asymmetries are often more pronounced in the gaseous component of galaxies, as it extends further than the stellar component. A key driver of morphological and kinematic disturbances that results in asymmetries are galaxy interactions with their environments and neighbours (Kereš et al. 2002; Fernández Lorenzo et al. 2013; Mundy et al. 2017). From both observations and modelling of the stellar and gas components of galaxies, it has been seen that galaxy-galaxy interactions and mergers (Reichard et al. 2008), galaxy-environment interactions (Angiras et al. 2006; van Eymeren et al. 2011), ram-pressure stripping, (Gunn & Gott 1972) and gas accretion from the cosmic web (Bournaud et al. 2005) can all drive morphological and kinematic asymmetries. The relative importance of these processes in different environments and at different epochs is not yet understood and is still an open question in the field of galaxy evolution. Studying the stellar and gas asymmetries of galaxies in these

different environments will help to provide information on the processes driving their evolution.

Various photometric techniques have been developed over the years to quantify two-dimensional (2D) morphological asymmetries based on galaxy stellar light distributions. The most well-known are the concentration-asymmetry-smoothness (CAS) parameters (Trujillo et al. 2001; Conselice 2003), the M_{20} parameter, and the G_{ini} coefficient (Lotz et al. 2004). These statistics were initially designed to develop a non-parametric set of classifications for 2D images. Conselice et al. (2000) found that a combination of color and asymmetry could be used to distinguish between spirals, ellipticals, and edge-on galaxies. Conselice (2003) followed up on this work and found that these morphological statistics correlate with important physical features. The concentration correlates with B/T ratios, smoothness tends to measure H α equivalent widths, and asymmetry can identify galaxies undergoing major mergers.

The idea of using morphological statistics as a classification method has been used in a variety of different areas. For instance, asymmetry has been used to find merging galaxies in Integral field unit (IFU) spectroscopy surveys of objects at intermediate to high redshift (Shapiro et al. 2008; Bloom et al. 2017, 2018; Wisnioski et al. 2019).

The cold gas component, in particular the neutral hydrogen, HI, in galaxies is also important to take into account when investigating the effects of galaxy interactions.

* E-mail: nathan.deg@ast.uct.ac.za

Typically, in disk galaxies, the HI is a significant fraction of the total mass of the galaxy and also has a more extended radial profile than the stellar component. Due to its nature and more extended radial distribution, the gas is therefore more susceptible to disruption on earlier timescales in galaxy-galaxy interactions than the stellar component of a galaxy. Asymmetries in the HI distribution and kinematics may also be caused by accretion of gas onto galaxies from the cosmic web and/or galactic fountain processes (for a review of HI accretion in galaxies see [Sancisi, et al. \(2008\)](#)).

[Kornreich et al. \(2000\)](#) investigated the asymmetries of 9 face-on spiral galaxies based on HI imaging data using several different techniques. More recently, various groups ([Holwerda et al. 2011](#); [Lelli et al. 2014](#); [Giese et al. 2016](#)) have applied quantitative methods similar to those employed in optical studies to measure the 2-D asymmetries of galaxy HI images. However, sample sizes of existing HI galaxy imaging surveys are of the order of at most a few hundred galaxies and are limited to the local Universe. For instance, the Westerbork HI survey of Irregular and SPiral galaxies (WHISP) has a catalogue of 375 galaxies ([van der Hulst, van Albada & Sancisi 2001](#)). Compared to optical surveys, the sample sizes of HI imaging surveys are much smaller and the redshift coverage has been constrained to the local Universe due to the extremely long observing times required for radio observations on interferometers (although upcoming surveys using MeerKAT and ASKAP will soon provide large numbers of resolved HI images). Single-dish surveys on the other hand, for example, HIPASS ([Meyer et al. 2004](#)) and ALFALFA ([Haynes et al. 2018](#)), have observed the global HI profiles of thousands of galaxies.

Typically HI profiles are characterized by three numbers; the integrated HI flux, the systemic velocity, and the profile width. Asymmetry gives at least one new statistic that can be used to characterize galaxies. Galaxy HI asymmetries have to date typically been measured in a range of different environments in the local universe using the galaxies' HI profiles. In 1974, [Peterson & Shostak \(1974\)](#) measured the asymmetry of the HI profiles of a sample of galaxies from the *Atlas of Peculiar Galaxies* by [Arp \(1966\)](#) and found that the HI profile asymmetries correlated with the optical morphological asymmetries they observed. Since then, many studies have measured HI profile asymmetries based on single-dish data; [Tift & Cocke \(1988\)](#) characterised HI profiles observed with the 91 m NRAO telescope at Greenbank and reported asymmetries calculated as a ratio of velocity differences between the edges of a profile and the velocity value resulting in equal area on each side under the profile. By analysing a large sample of ~ 1700 mostly field galaxy HI profiles, by eye, [Richter & Sancisi \(1994\)](#) concluded that approximately half of galaxies have asymmetric HI profiles. Using the Green Bank 43m telescope [Haynes et al. \(1998\)](#) observed the HI profiles of 78 isolated spiral galaxies and used two quantitative methods to measure the profile lopsidedness. Classifying profiles as lopsided if the difference in area under the profile on each side of the median systemic velocity was greater than 5 percent resulted in a similar asymmetry rate of ~ 50 percent for their sample. [Matthews et al. \(1998\)](#) found a ~ 77 percent HI profile asymmetry rate in their sample of 30 late-type spirals and also found a generally higher rate of asymmetry in the HI profiles compared to the optical images for their sample.

More recently, [Espada et al. \(2011\)](#) set out to measure the HI profile lopsidedness distribution of extremely isolated galaxies in the AMIGA (Analysis of the Interstellar Medium of Isolated GALaxies) sample¹ in order to estimate a baseline intrinsic asymmetry rate against which other samples in different environments could be compared. They used the same quantitative technique of comparing the integrated flux ratios on each side of the median systemic velocity. Fitting a half-Gaussian distribution to their data resulted in a standard deviation of $\sigma = 0.13$ and galaxies were classified as asymmetric if their lopsidedness values deviated by more than 2σ , i.e., had lopsidedness values $A > 1.26$. Using this asymmetry criterion, only 9 percent of the AMIGA HI-refined sample of 166 galaxies were found to be asymmetric and applying the same criterion to previous studies, they found a similar rate for the isolated [Haynes et al. \(1998\)](#) sample but a larger rate for the [Matthews et al. \(1998\)](#) field sample (see Table 3 in their paper ([Espada et al. 2011](#))).

To probe the impact of mergers on galaxy HI profile asymmetries, [Bok et al. \(2019\)](#) investigated the rate of lopsidedness in ALFALFA ([Haynes et al. 2018](#)) HI profiles of 348 galaxies in close pairs (an optical neighbour within 100 kpc and 500 km s^{-1}) identified in the Sloan Digital Sky Survey DR7 ([Abazajian 2009](#)) using the same flux ratio method. Based on the [Espada et al. \(2011\)](#) asymmetry criterion, they found a significantly higher asymmetry rate (27 percent) in their close pair sample compared to the isolated and field samples of [Espada et al. \(2011\)](#), [Haynes et al. \(1998\)](#), and [Matthews et al. \(1998\)](#) and their own field sample (18 percent), indicating statistically that merger activity is a driver of HI profile lopsidedness.

[Watts et al. \(2020\)](#) recently examined a sample of 562 galaxies from the extended GALEX Arecibo SDSS Survey (xGASS) ([Catinella et al. 2010, 2018](#)). They also found that environment was a key driver of asymmetries, with satellite galaxies having a higher rate of asymmetry than central galaxies, and that isolated centrals had slightly higher symmetry than group centrals. Interestingly, they also found that asymmetric galaxies in their sample typically had a lower gas fraction than symmetric galaxies.

In the near future, thousands of galaxy HI images are expected to be available from SKA precursor shallow HI surveys such as WALLABY ([Duffy et al. 2012](#)) on ASKAP and MIGHTEE ([Jarvis et al. 2016](#)) on MeerKAT. However, the deeper HI surveys such as DINGO ([Duffy et al. 2012](#)) on ASKAP and LADUMA ([Blyth et al. 2016](#)) on MeerKAT that are aiming to observe HI in galaxies far beyond the local universe, will not spatially resolve the HI disks of higher redshift galaxies. An interesting aspect of asymmetry measurements is, due to the channel resolution being roughly equal at low and intermediate redshifts ($z \sim 0$ and $z \sim 0.5$ respectively), a direct comparison of profile asymmetries at various redshifts is possible. Moreover, just as the 2D morphological statistics can be used to classify galaxies ([Conselice 2003](#)), it may be possible to classify profiles with a full suite of different asymmetry measurements. While most of the methods (including those presented in this paper) used to quantify 2D and 1D asymmetries in galaxies are non-parametric, it is also possible to extract asymmetry measures by fitting HI

¹ <http://amiga.iaa.es>

global profiles with physically motivated models (e.g. [Stewart, Blyth & de Blok \(2014\)](#)) or parameterised functions (e.g. the ‘Busy function’ [Westmeier, et al. \(2014\)](#)). Since parametric methods have not yet been broadly applied in the literature, we focus rather on comparisons to non-parametric methods here.

In this paper, with both the upcoming HI datasets from the SKA pathfinders and the idea of characterizing velocity profiles with multiple statistics in mind, we introduce two new asymmetry statistics. One of these is a 1D analogue of the 2D asymmetry statistic, while the other is similar to the velocity method given by [Haynes et al. \(1998\)](#), but is derived from the profile lopsidedness. We examine how these depend on a variety of observational effects using mock profiles and numerical simulations. We also calculate these statistics for the WHISP sample and compare them to a visual classification of the profiles.

In Section 2 we present statistics for quantifying velocity profiles. Section 3 explores the dependence of these statistics on the ‘folding’ velocity and the S/N using mock test profiles. Section 4 presents two simulations of interacting galaxy pairs. These are used to explore how the various statistics depend on the observed viewing angle and inclination. Next, in Sec. 5, we apply these statistics to a sample of galaxies from the WHISP survey. Finally, Sec. 6 presents our discussion and conclusions about these statistics.

2 MEASURES OF ASYMMETRY

Compared to the variety of two-dimensional methods, there are considerably few statistics for analyzing 1-D velocity profiles. The most common is the lopsidedness statistic which compares the flux in the approaching and receding portions of a particular velocity profile (e.g. [Haynes et al. \(1998\)](#)).

It is important to make a few notes on terminology here. Typically lopsidedness and asymmetry are used interchangeably when discussing velocity profiles. In this work we will introduce other asymmetry statistics so we will exclusively call the usual statistic lopsidedness. One of the other statistics that we will introduce involves a channel-by-channel comparison of fluxes that is similar in construction to the 2-D asymmetry statistic. For the sake of comparison we will refer to that statistic as the channel-by-channel asymmetry or as the asymmetry statistic.

In addition, this work uses a variety of different characteristic velocities that are introduced throughout the paper. To that end, Table 1 summarizes the different velocity measures along with where they are defined.

2.1 Lopsidedness

The lopsidedness statistic compares the integrated flux on either side of some ‘folding’ velocity, v_{fold} . It is typically set equal to the systemic/median velocity of the galaxy, v_{sys} . In the literature the lopsidedness is most often calculated (e.g. [Haynes et al. \(1998\)](#); [Espada et al. \(2011\)](#); [Bok et al. \(2019\)](#)) as

$$A_{L,r} = \max\left(\frac{H}{L}, \frac{L}{H}\right), \quad (1)$$

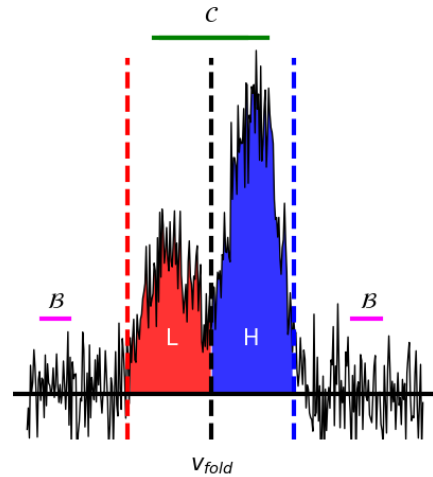


Figure 1. A graphical explanation of the lopsidedness and asymmetry statistics. The lopsidedness compares the red and blue areas. The lopsidedness can be set to either the maximal ratio of L and H , $A_{L,r}$ or to the normalized difference between the two, A_L . The channel-by-channel asymmetry statistic, \mathcal{A} compares the difference between pairs of matched channels, which are then summed to C . A similar number of channels beyond the range of the profile are also compared to get B , which is then subtracted from C to get \mathcal{A} . The dashed red and blue vertical lines indicate the edge of the velocity profile while the dashed black line indicates the folding velocity used for the calculation of A_L and \mathcal{A} .

where $A_{L,r}$ is the lopsidedness ratio and L and H are the integrated flux on the low/high side of the profile respectively. Explicitly, this is

$$L = \int_{v_{low}}^{v_{fold}} f(v)dv, \quad (2)$$

and

$$H = \int_{v_{fold}}^{v_{high}} f(v)dv, \quad (3)$$

where $f(v)$ is the flux density as a function of velocity and v_{fold} is the velocity separating L from H . Figure 1 shows a sample velocity profile to illustrate the lopsidedness statistic.

The limits on Eq. 1 are formally one and infinity, where one is perfectly symmetric and infinity is completely lopsided. In practice, a lopsidedness of two or more is quite extreme. However, the 2-D analogues of lopsidedness have limits between zero and one. As such, we prefer the definition of lopsidedness developed by [Peterson & Shostak \(1974\)](#). In their definition,

$$A_L = \frac{|L - H|}{L + H}. \quad (4)$$

In this formulation, $0 \leq A_L \leq 1$, where $A_L = 0$ is perfectly symmetric. It is straightforward to convert between Eq. 1 and 4 using

$$A_L = \frac{A_{L,r} - 1}{A_{L,r} + 1}. \quad (5)$$

In terms of true dynamical range, $A_L = 0.33$ corresponds to a flux ratio of 2, which, as mentioned earlier, is very asymmetric.

Symbol	Location	Definition
v_{low}	Sec. 2.1	The smallest velocity in the profile given the chosen width.
v_{high}	Sec. 2.1	The highest velocity in the profile given the chosen width.
v_{fold}	Sec. 2.1	The velocity used to separate the lower portion of the profile from the higher when calculating various asymmetry statistics.
v_{sys}	Sec. 2.2	The systemic velocity defined as the midway point between v_{low} and v_{high} .
v_{equal}	Sec. 2.2	The value of v_{fold} that gives zero lopsidedness.
$v_{l,i}$	Sec. 2.3	The low velocity channel for a velocity pair.
$v_{h,i}$	Sec. 2.3	The high velocity channel for a velocity pair.
v_{sym}	Sec. 3.1	The folding velocity that minimizes \mathcal{A} .

Table 1. A list of the different velocities used in this work.

2.2 Velocity of Equality

Typically the lopsidedness statistic is calculated at the systemic velocity of the profile. To be clear, the systemic velocity we use is $v_{sys} = (v_{high} - v_{low})/2$ where v_{high} and v_{low} are the edge velocities, which in turn are defined by the peak to edge flux ratio (see Sec. 2.4). For single peaked profiles $F(v_{low\ peak}) = F(v_{high\ peak})$, but for double horned profiles, these fluxes can be different.

That being said, in every profile there exists a folding velocity such that $A_L(v_{equal}) = 0$, where v_{equal} is the ‘velocity of equality’. This velocity can be used to define a new statistic, ΔV . This is the difference between the systemic velocity and the velocity of equality normalized by the width of the profile. Explicitly, this is

$$\Delta V = \frac{2|v_{sys} - v_{equal}|}{w}, \quad (6)$$

where w is the width of the velocity profile (defined by the profile edges). The factor of 2 is introduced so that the formal limits on this statistic are $0 \leq \Delta V \leq 1$, but generally the magnitude will be significantly smaller.

Our ΔV statistic is very similar to how Haynes et al. (1998) used differences between the flux-weighted mean velocity, \bar{v} , and the systemic velocity to characterize profile asymmetries. The key difference between our two methods is that $v_{equal} \neq \bar{v}$. The flux-weighted mean velocity does not always coincide with the velocity where the lopsidedness is zero. While the two statistics are similar, we use ΔV in this work as it is explicitly connected to A_L through v_{equal} .

It is worth noting that the asymmetry statistic used by Tift & Cocke (1988) also uses v_{equal} , but the formulation is quite different than our ΔV . They examine the ratio of $(v_{equal} - v_{low})$ and $(v_{high} - v_{equal})$ and v_{sys} is only included to give the sign and determine which factor will be the numerator or denominator. It is closer in construction to Eq. 1 than Eq. 6.

2.3 Channel-by-Channel Asymmetry

The lopsidedness statistic is a relatively global statistic. It is an integral quantity that compares the total flux on either side of some central velocity. However, the 2-D asymmetry statistic is much more local (Conselice et al. 2000). The 2-D asymmetry is

$$\mathcal{A}_{2D} = \frac{\sum_i |f_i - f_{180,i}|}{2 \sum_i f_i}, \quad (7)$$

where f_i is the flux of a pixel and $f_{180,i}$ is the flux of the pixel located at 180° rotation from the i 'th pixel. The factor of 2 in the denominator is present to deal with double-counting.

The difference between the integrated lopsidedness and the more local 2-D asymmetry has, in part, motivated the development of a new channel-by-channel 1-D asymmetry statistic, \mathcal{A} . Related to this motivation is the fact that lopsidedness integrates out small, dynamically local variations in the velocity profile. These variations may contain subtle information about the galaxy that lopsidedness will not detect.

The channel-by-channel asymmetry (or 1-D asymmetry due to its similarity to the 2-D asymmetry) is the normalized sum of flux differences across v_{fold} . Because this quantity is local, it may be strongly affected by background noise. As such, we calculate a background term and subtract it from the summation in the signal region to obtain the measured asymmetry. Explicitly

$$\mathcal{A}_{meas} = \mathcal{C} - \mathcal{B} \quad (8)$$

where \mathcal{C} is the degree of asymmetry in the profile, while \mathcal{B} is the amount of asymmetry due to noise. The signal term is

$$\mathcal{C} = \frac{\sum_i |f(v_{l,i})\delta v - f(v_{h,i})\delta v|}{\sum_i ((f(v_{l,i})\delta v + f(v_{h,i})\delta v))}, \quad (9)$$

where $v_{l,i}$ and $v_{h,i}$ are the i 'th velocity pair and δv is the channel width. They are given simply by $v_{(l,h),i} = v_{sys} \pm (i \times \delta v)$. The background term is similar to the profile term except it is still normalized by the total flux density of the velocity profile. That is

$$\mathcal{B} = \frac{\sum_i |f(v_{b,l,i})\delta v - f(v_{b,h,i})\delta v|}{\sum_i (f(v_{l,i})\delta v + f(v_{h,i})\delta v)}, \quad (10)$$

where $f(v_{b,i})$ is the flux density in some channel outside the velocity profile. Figure 1 shows the location of \mathcal{C} and \mathcal{B} relative to a sample velocity profile.

By construction, the limits on \mathcal{C} and \mathcal{B} are between zero and one. Since \mathcal{A} is the difference of the signal and background terms, it is possible for it to be negative. This implies that the profile is noise dominated and a channel-by-channel asymmetry measurement cannot be made reliably.

The 1-D asymmetry and lopsidedness statistics are similar in both construction and range, but they measure different things. While both statistics are calculated on the global HI profile, the channel-by-channel asymmetry is sensitive to ‘local’ perturbations (where local refers to specific velocity channels). Lopsidedness is more sensitive to larger scale perturbations to the velocity profile.

As a thought experiment, it is possible to imagine observing a ‘real’ galaxy using an instrument with infinite velocity resolution and no noise. The galaxy will have a symmetric double horned profile with zero lopsidedness. For there to be zero channel-by-channel asymmetry the infinite resolution of the instrument requires that the galaxy consist of symmetrically arranged gas clouds such that each approaching cloud is paired with a receding cloud with equal and opposite velocity relative to v_{sys} . In a ‘real’ galaxy, gas clouds are drawn from a distribution function and such pairs are unlikely. Instead this galaxy ‘observation’ would tend towards having $\mathcal{A} = 1$ as each channel pair would contain the flux of a single gas cloud (again, this is due to the infinite resolution and discretized gas clouds). This is a contrived example, but it illustrates that the lopsidedness and channel-by-channel asymmetry statistics measure different things.

2.4 Implementation

We have implemented our profile analysis using custom PYTHON code. The code itself uses the standard NUMPY package for most array calculations. In some later steps, we utilize the LMFIT (Newville et al. 2014) PYTHON package to calculate the ‘velocity of symmetry’ (see Tab. 1 and Sec. 3 for details).

The lopsidedness integrations are performed using a modified trapezoid integral that can account for unequal channel spacings. This is necessary as neither the edges nor v_{fold} may lie directly on a particular channel value.

The calculation of v_{equal} for ΔV uses a simple bisection rootfinder on a version of Eq. 4 that does not include an absolute sign. The ‘signed’ lopsidedness has limits of one and negative one and passes through zero at v_{equal} .

The channel-by-channel asymmetry is calculated by taking pairs of v_i in equal outward steps of δv from v_{fold} . When v_{fold} does not lie on a channel, we use linear interpolation to find the flux values for each v_i in Eq. 9.

More importantly, a technical issue arises when $v_{fold} \neq v_{sys}$. \mathcal{A} requires an equal number of channels on either side of v_{fold} . In order to include the entire profile, it is necessary to consider channels beyond the edge. In other words the width considered, w_A , is

$$w_A = 2\max(v_{fold} - v_{low}, v_{high} - v_{fold}) , \quad (11)$$

and is centered on v_{fold} .

As a note, in the rest of this work, we define the profile edges as the velocities where the flux equals 20% of the peak flux or fluxes for single or double peaked profiles respectively.

3 MEASUREMENT SYSTEMATICS

In order to test the dependence of the lopsidedness and asymmetry statistics on the folding velocity, signal-to-noise, and resolution, we have generated a set of mock velocity profiles from the sums of Gaussian functions. Since these profiles are simple and noise free, they allow for an isolation of the effect of the folding velocity. The set of profiles consists of a single-peaked Gaussian, G , a symmetric double-peaked profile, S , a profile that is slightly asymmetric, SA , a very asymmetric profile, VA , and a fifth profile that has one broad low-flux peak and one thin high-flux peak, BT .

3.1 Dependence on Folding Velocity

Figure 2 shows the lopsidedness and asymmetry statistics as a function of v_{fold} . As noted in the discussion of v_{equal} , A_L always has a minimum of zero. This does not always occur at v_{sys} , leading to our proposed ΔV statistic.

It is abundantly clear in Fig. 2 that the channel-by-channel asymmetry statistic (shown in black) has a different profile than the lopsidedness (shown in red). In all the double-peaked profiles, there is one global minimum, and, for the double peaked profiles, two local minima that occur at the locations of the peaks. These local minima occur due to the symmetry of the peaks cancelling out pairs near those values of v_{fold} .

Unlike the lopsidedness, the asymmetry statistic has a unique minimum for each profile. In our simple test cases this minimum usually occurs at v_{sys} . However, in the BT profile, this minimum is different than v_{sys} . As such, we consider two versions of the asymmetry statistic. The first is calculated at v_{sys} that can be easily compared to the lopsidedness. The second is calculated at the ‘velocity of symmetry’, v_{sym} , (like the center of symmetry in 2-D images). At this velocity, the asymmetry is minimized removing some of the uncertainty in the calculation of \mathcal{A} that would arise due to uncertainties in calculating v_{sys} . Moreover, since the system itself may not be in equilibrium, the relation between a calculation of v_{sys} and the true velocity of the entire galaxy is not quite always clear. In practical terms we find the velocity of symmetry using the LMFIT (Newville et al. 2014) PYTHON package. For simplicity we will use \mathcal{A} for the 1-D asymmetry at the ‘velocity of symmetry’ and $\mathcal{A}(v_{sys})$ when calculated at the systemic velocity.

3.2 Dependence on Profile Signal-to-Noise Ratio

These profiles are also useful for exploring the effect of the signal-to-noise ratio, S/N , on the measured statistics. We generated profiles with a specific peak S/N by first calculating the noise, σ . The noise is found by dividing the peak flux by the target S/N . Then a random value is drawn from a Gaussian distribution centered at zero with a dispersion equal to σ in all velocity channels and added to the profile. In order to get robust results we generated 100 bootstrap samples for each profile at each S/N value. Fig. 3 shows the average values and $1-\sigma$ error bars from those samples.

The effect of the noise on the lopsidedness is quite interesting for two reasons. Firstly, the value of A_L decreases as a function of S/N to some asymptotic value. Secondly, and much more interestingly, the asymptotic value is quite different for the VA and BT profiles. While the two profiles appear to be nearly as asymmetric by eye, the lopsidedness of the BT profile is close to zero. The low lopsidedness for the BT profile is due to the fact that the broad and narrow peaks have nearly the same amount of flux on either side of v_{sys} . Therefore, while the profile may appear to be asymmetric, the asymmetries are local and there is no overall lopsidedness.

The ΔV statistic is more similar to the lopsidedness than the asymmetry. It is unsurprising that the two quantities are so similar, as ΔV depends on A_L . However, in the SA case, ΔV is the largest statistic for most S/N values. The key point here is that ΔV is not just a reformulation

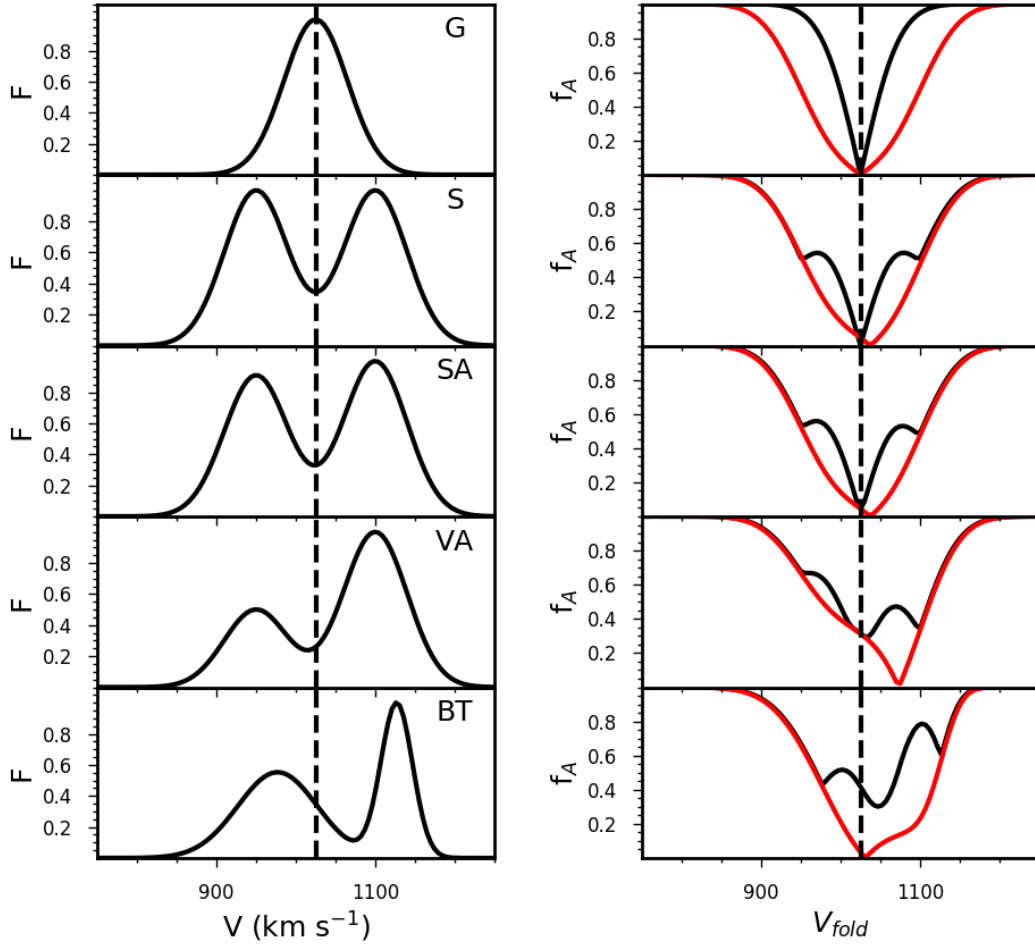


Figure 2. Normalized test velocity profiles (left panels) and the asymmetry (black lines) and lopsidedness (red lines) statistics as a function of v_{fold} for each profile (right panels). The five velocity profiles are a Gaussian profile, G , a symmetric double peaked profile, S , a slightly asymmetric double-peaked profile, SA , a very asymmetric double-peaked profile, VA , and a profile with one broad peak and one thin peak, BT .

of A_L and gives different information about the profile than the lopsidedness.

The channel-by-channel asymmetry exhibits a different behaviour. Both C and B decrease as a function of S/N , but the rate of decrease between these values differs. Because the decrease in B is smaller than C , A increases to some asymptote. Ultimately, the background subtraction means that A is a measurement of how much asymmetry may be robustly attributed to the signal. C includes both contributions from the underlying signal and the noise. In principle, B calculates the amount of the asymmetry that could arise due to random noise. When the noise is large it can dominate over the asymmetry due to the signal. While there may be more ‘asymmetry’ in the noise-free profile, it is impossible to definitively attribute it to the signal if the profile is noisy.

It is worth noting that in the BT case $A(v_{sys})$ is sig-

nificantly higher than A . This makes sense as Fig. 2 shows that only in the BT case is v_{sym} significantly different than v_{sys} . This result highlights the importance of calculating the minimal asymmetry.

In summary, Fig. 3 shows that the lopsidedness and ΔV statistics reach an asymptotic value at lower S/N values than the channel-by-channel asymmetry measurement. However, the channel-by-channel asymmetry is still large for the visually asymmetric BT profile where the lopsidedness and ΔV are roughly zero. This result emphasizes that these different asymmetry statistics quantify different effects. As such, when analyzing a particular profile, all the statistics should be measured. However, it is also important to account for biases that may arise due to the S/N when comparing different objects.

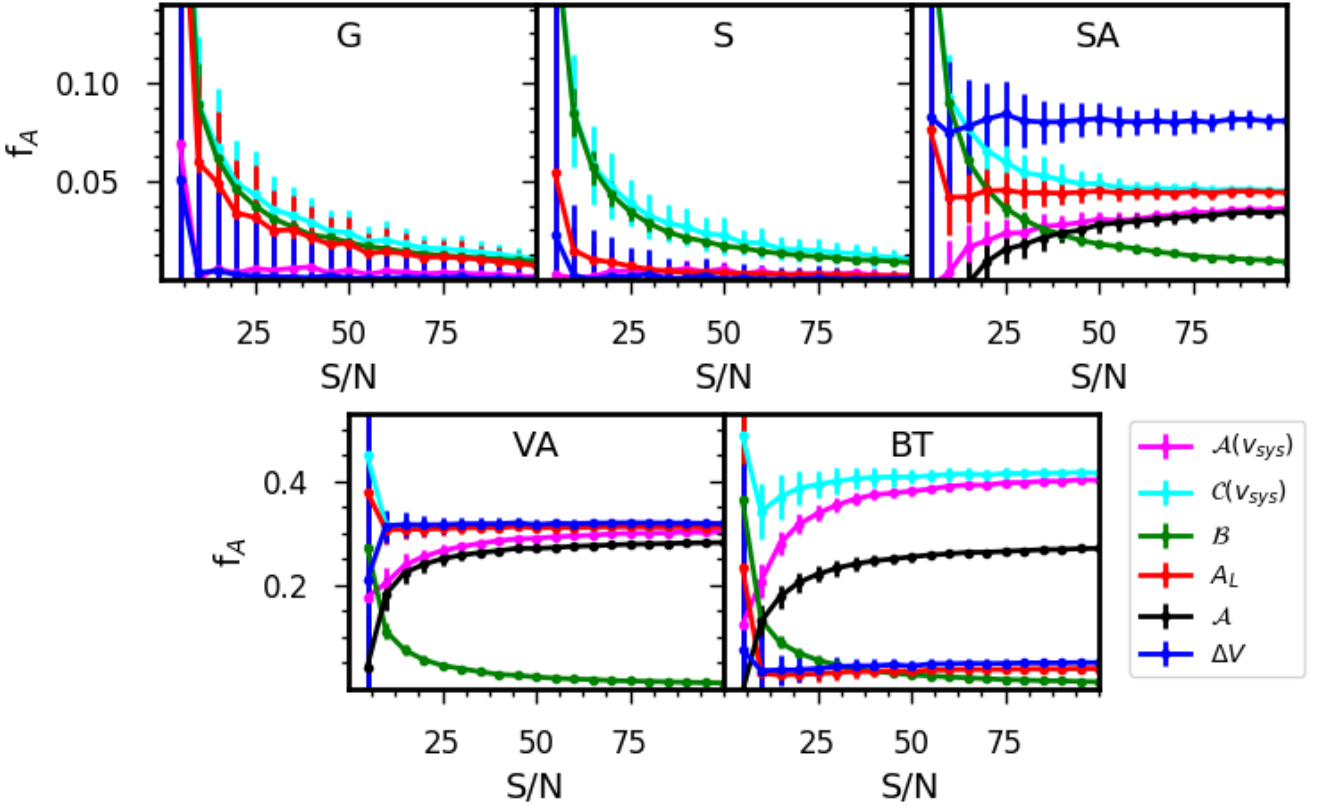


Figure 3. The asymmetry and lopsidedness statistics for the five velocity profiles as a function of S/N . The magenta and red curves are the asymmetry and lopsidedness measured at v_{sys} . The cyan and green curves are the average C and B terms used to calculate \mathcal{A} . The black curve is the asymmetry statistic calculated at the ‘velocity of symmetry’. Finally, the blue curve is the ΔV statistic. The points and error bars for each statistic were calculated from 100 realizations of the velocity profiles at each S/N ratio.

3.3 Dependence on Profile Velocity Resolution

One potential issue with the channel-by-channel measures is the dependence on the resolution of the HI profile. To that end, Fig. 4 shows the average asymmetry statistics for a variety of resolutions and S/N ratios. For simplicity, this plot only shows the calculations for the symmetric, S , and very asymmetric, VA , profiles. As with the S/N tests, we generated 100 realizations with its own random noise for each profile and plot the average values with dispersions indicated by the error bars on the data points.

Before discussing the resolution effects, it’s worth noting that, for all S/N values, $\mathcal{A} < 0$ for the S profile. This would also have been apparent in Fig. 3, except the limits were set to zero in that plot. We highlight this here to demonstrate how symmetric or nearly symmetric profiles can have \mathcal{A} below zero. As noted in Sec. 2.3, when the profile is symmetric the background subtraction can reduce a positive C below zero.

For both the S and VA profiles, a steady value for all the asymmetry parameters is reached for all S/N , for all resolutions above ~ 20 channels. For profiles with fewer than 20 channels, the dispersions for all the asymmetry parameter measurements increase substantially as seen by the increase

in the size of the error bars. Most notable is the effect on ΔV where the scatter is largest. For most of the asymmetry statistics, once the number of resolution elements drops below ~ 20 , the mean values of the measured statistics also drop, resulting in an under-estimate of the true asymmetry. An exception is the case for the lopsidedness, A_L , which actually increases in the case of a symmetric profile, therefore over-estimating the true asymmetry. In all cases, with increasing S/N , the effect of reduced resolution is minimized. In conclusion, the number of channels which an HI profile spans is important to take into account when measuring the different asymmetry parameters, particularly when the S/N of the profiles is low. For higher S/N profiles, one can measure the asymmetry reliably at lower resolutions down to ~ 15 channels. The parameter most susceptible to resolution effects is the ΔV statistic.

4 SIMULATIONS

In order to understand how the four asymmetry statistics depend on viewing angle and inclination, we utilize two simulations of merging galaxies. The galaxies are generated using the GALACTICS code (Deg et al. 2019) and the com-

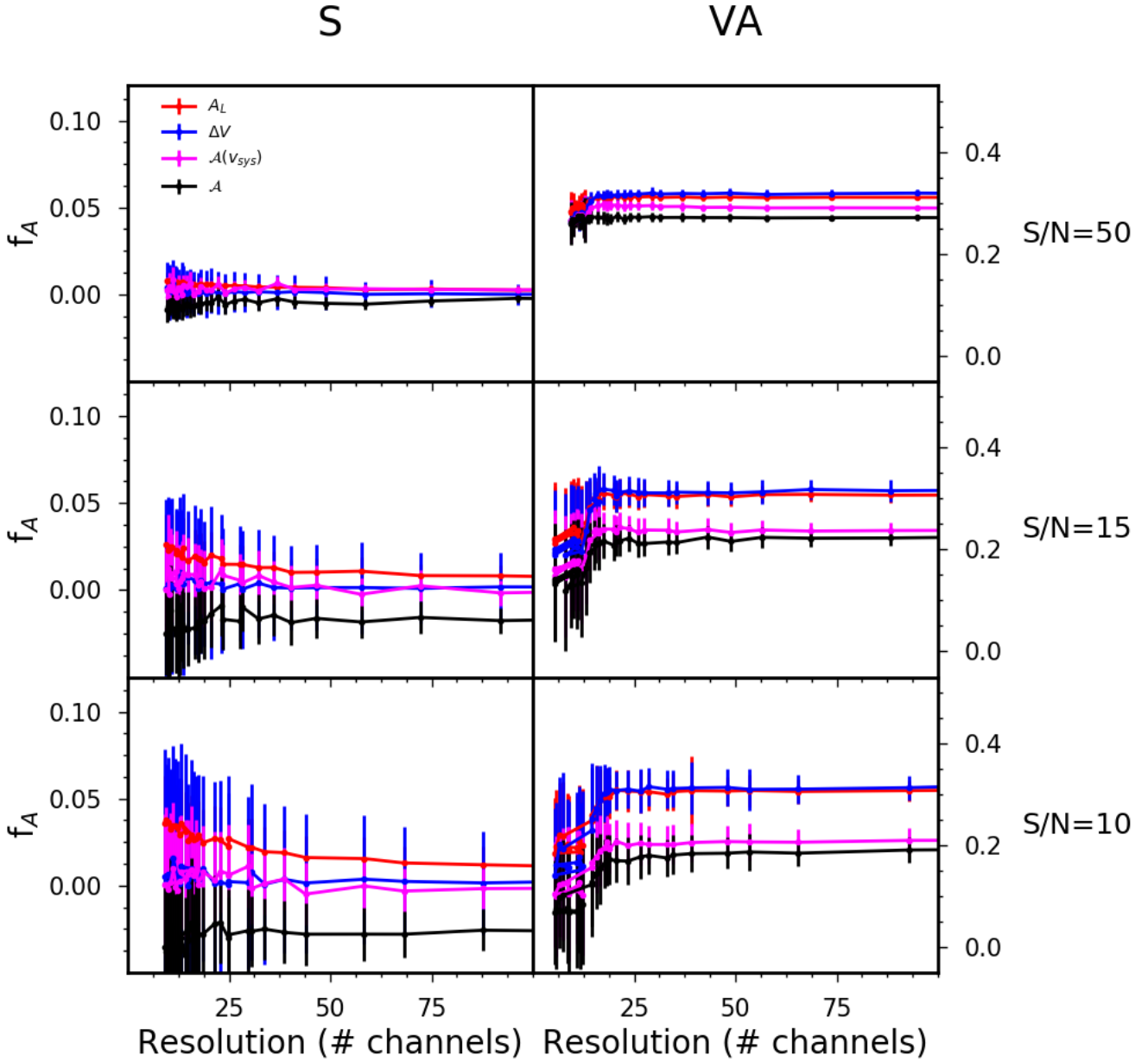


Figure 4. The resolution and S/N dependence for the different asymmetry statistics. The black, magenta, red, and blue lines are the average \mathcal{A} , $\mathcal{A}(v_{sys})$, A_L , and ΔV statistics for 100 bootstrap samples respectively. The resolution is the number of channels contained within the profile.

binned systems are evolved using the Gadget-2 N-body code (Springel 2005). We then analyze the profile generated from a single galaxy at a variety of viewing angles and inclinations.

4.1 Simulation Details

We utilize the GALACTICS code to generate the initial conditions for the simulations. The full details of the code are described in Deg et al. (2019). In brief, GALACTICS gener-

ates equilibrium galaxy models that may consist of a Sérsic bulge, a double-power law dark matter halo, up to two exponential-sech² stellar disks, and an exponential surface density gas disk.

We have run two simulations of merging galaxies in order to explore the effects of viewing angle and inclination on the various asymmetry statistics. The first simulation, called the ‘Shock Sim’ has the two galaxies crash into each other directly. The second simulation, called the ‘Fly-by Sim’ has the two merge over the course of a more gentle interaction.

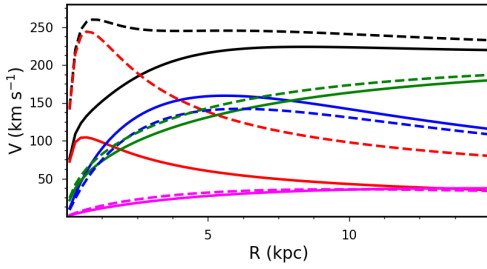


Figure 5. The rotation curves for the Shock Sim (dashed lines) and Fly-by Sim (solid lines). The black lines are the total rotation curves, while the red, blue, magenta, and green lines are the bulge, stellar disk, gas disk, and halo contributions respectively.

Fig. 5 shows the initial rotation curves for each model. Each galaxy in the Shock Sim has 10^5 gas particles, 10^5 bulge particles, 2×10^5 disk particles, and 10^6 halo particles. Each galaxy in the Fly-by Sim has 2×10^5 gas particles, 10^5 bulge particles, 5×10^5 disk particles, and 10^6 halo particles.

In both simulations, one galaxy is placed at $(\mathbf{x}, \mathbf{v}) = (0, 0)$. For the Shock Sim, the second galaxy is initialized at $\mathbf{x} = (0, 300, 0)$ kpc, $\mathbf{v} = (0, -25, 0)$ km s $^{-1}$. There is no global rotation of the second galaxy, making the interaction edge-on and producing a strong shock during the initial encounter. In the Fly-by Sim, the second galaxy begins at $\mathbf{x} = (85, -67, 27)$ kpc, $\mathbf{v} = (64, 320, -14)$ km s $^{-1}$ and is rotated so that the initial inclination 45° relative to the $X - Y$ plane. This produces a slower, fly-by first passage that then merges together over later passages.

Both systems are evolved using GADGET-2 for 5 Gyr. The simulations use an adaptive softening length of with a maximum length of 0.5 kpc. The Courant factor used in this simulation is 0.25. In order to have significant time resolution, snapshots are produced every 0.005 Gyr.

We have chosen a single snapshot from each simulation for analysis. For the Shock Sim, the snapshot is at $T = 1.93$ Gyr, while for the Fly-by Sim we use the $T = 2.5$ Gyr snapshot. For simplicity we only analyze the gas particles that initially belong to a single galaxy in that snapshot. Figure 6 shows the surface density maps selected for analysis. The Shock Sim shows a clear shock wave at the interaction interface and the Fly-by Sim shows large tidal tails. A consequence of this is that some of the particles selected for analysis have been captured by the second galaxy. This selection is not realistic, but it is sufficient accurate for our focus on asymmetry statistics. Future work will examine the effect of properly separating the different galaxies from an observational point of view.

4.2 Mock Observations

We have generated mock observations of the Shock Sim and Fly-by Sim at a variety of viewing angles and inclinations. The selected particles from a particular snapshot are rotated using Euler angles, and then shifted to a new center. Changing the Euler angles changes the viewing angle and inclination of the galaxy. A systemic velocity of 1000 km s $^{-1}$ is then added to each galaxy. From this new position and velocity, v_r is calculated for an observer.

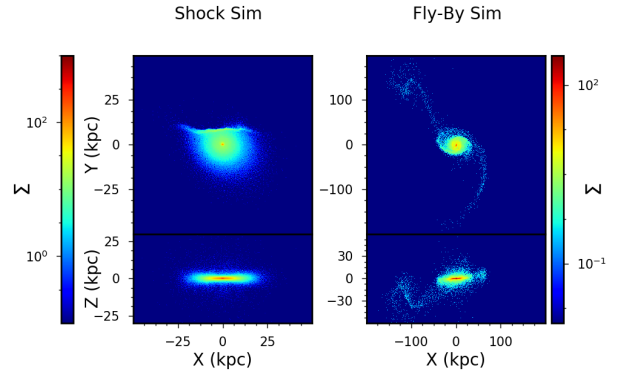


Figure 6. The gas disk surface density of the analyzed galaxy for the Shock Sim (left) and Fly-by Sim (right). The Shock Sim surface density is calculated at $T = 1.93$ Gyr and the Fly-by Sim is calculated at $T = 2.5$ Gyr. The surface density units are $M_\odot \text{pc}^{-2}$.

To construct velocity profiles, we use 800 channels with a velocity resolution of 5 km s $^{-1}$. The luminosity of each particle is convolved with a Gaussian profile with $\sigma = 15$ km s $^{-1}$ and added to each channel.

4.3 Viewing Angle

Nature only gives us a single viewing angle and inclination for any particular interaction. However, with a simulation, it is possible to vary these parameters and explore how they affect the measurement of some quantity of interest, in this case the asymmetry.

Figure 7 shows the dependence of the four asymmetry statistics \mathcal{A} , A_L , ΔV , and $\mathcal{A}(v_{sys})$ as a function of viewing angle for the Shock Sim. Figure 8 shows the same quantities for the Fly-by Sim. For each of these plots, the observed galaxy has an inclination of 45° . It is worth noting that the sample images in Fig. 8 do not show the full extent of the tidal tails. However, the velocity profile includes the contribution of all the gas particles, whether they are in the main body, the tidal tail, or trapped in the second galaxy.

Firstly, the viewing angle affects all four asymmetry statistics. This is due to the fact that velocity profiles combine both kinematic and morphological information. The images and velocity profiles shown in Fig. 7 demonstrate this quite clearly. The image is approximately the same for each of the selected viewing angles, but the projection of the shock towards the observer changes. This projection causes the large variations in the observed velocity profiles.

The second thing to note in the two figures is that \mathcal{A} seems to be least sensitive of the statistics to viewing angle variations. This is especially clear in Fig. 7, where, for certain viewing angles like $\Theta = 95^\circ$, $\mathcal{A} = \Delta V = 0$. That specific profile is similar to our test ‘broad-thin’ profile, and the flux on either side of the systemic velocity is the same. At other angles, such as $\Theta = 290^\circ$, the lopsidedness and ΔV statistics are larger than \mathcal{A} . The first takeaway from this is that the viewing angle has a strong effect on the calculation of any asymmetry statistic. In some cases it is possible for a very

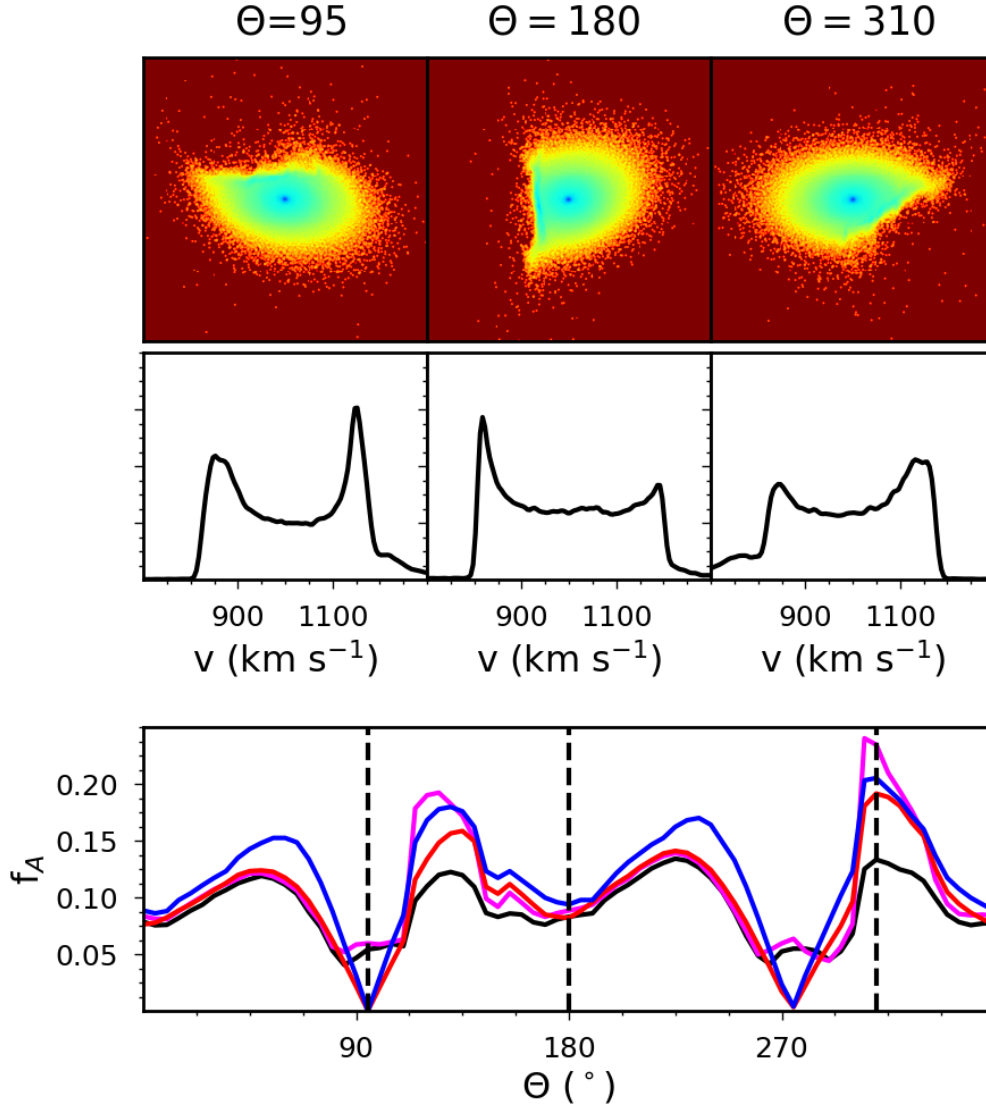


Figure 7. The asymmetry statistics for the Shock Sim as a function of viewing angle (bottom), along with a set of mock images (upper panels) and velocity profiles (middle panels) at specific viewing angles. The solid black, red, blue and cyan lines are \mathcal{A} , A_L , ΔV , and $\mathcal{A}(v_{sys})$ respectively, while the dashed vertical lines indicate the viewing angles of the images and velocity profiles shown in the panels above.

asymmetric galaxy image to have profiles with no global lopsidedness. Thus, while a lopsided profile almost certainly indicates some disturbance to the galaxy, low lopsidedness does not indicate an undisturbed galaxy. The second point is that \mathcal{A} is the most stable of the asymmetry statistics and it never indicates that the profile is symmetric due to its sensitivity to local perturbations in the profile.

A third interesting, but somewhat more minor, result is the sensitivity of the three statistics to the low flux ‘wings’ of the Shock-Sim profile. As the viewing angle changes a low flux feature moves through the channels. This feature is seen in the high velocity wing of the $\Theta = 95^\circ$ profile and at the low velocity wing of the $\Theta = 310^\circ$ profile. This feature is actually due to the projection of the shock velocity along the line-of-sight. The effect of this feature, and in particular, the wings, is somewhat subtle and may suggest another diagnostic for future work. When the shock wave creates a profile

wing it changes the estimate of v_{sys} due to our definition of the profile edges being the velocities that have 20% of the peak fluxes. The wings have enough flux at certain orientations to move the edge values and thereby change v_{sys} . This in turn strongly affects A_L , ΔV , and $\mathcal{A}(v_{sys})$. It has a much smaller effect on \mathcal{A} as that is calculated at v_{sym} . In Fig. 7 the orientations where the wings are included or skipped can be clearly seen by the jumps in A_L , ΔV , and $\mathcal{A}(v_{sys})$ at $\Theta = 115^\circ$ and $\Theta = 300^\circ$. In this work we have restricted ourselves to the 20% edge definition. At the 50% limits, the low flux wings would not affect the edge locations. As such, v_{sys} would be more stable with viewing angle and the shape jumps seen in the asymmetry statistics would not be seen. This suggests that a comparison of v_{sys} , A_L , ΔV , or $\mathcal{A}(v_{sys})$ calculated at both the 20% and 50% limits might be used to detect global profile wings. However, such a diagnostic would have to be used carefully due to the effects of noise in

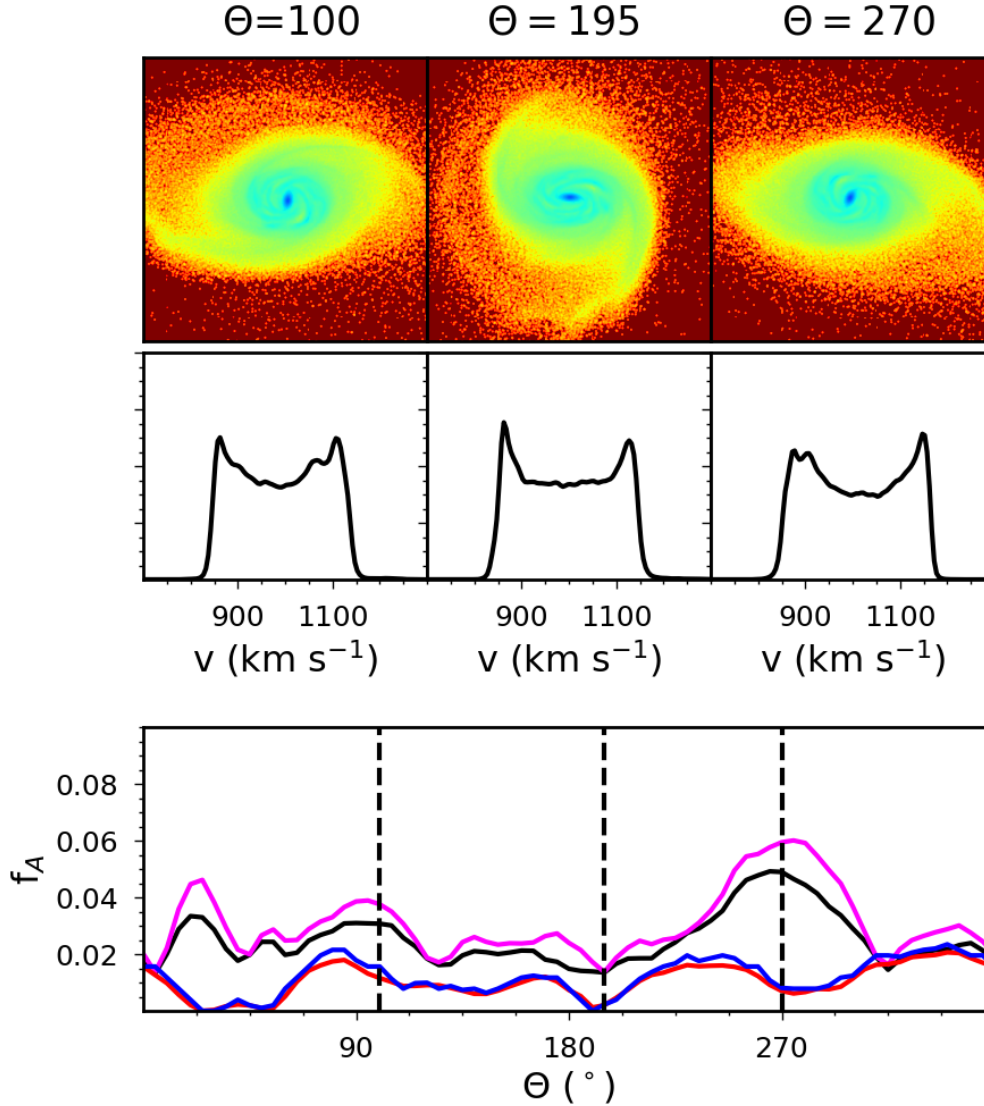


Figure 8. The asymmetry statistics for the Fly-by Sim as a function of viewing angle (bottom), along with a set of mock images (upper panels) and velocity profiles (middle panels) at specific viewing angles. The lines are the same as in Fig. 7.

more realistic measurements. This possibility is something that we will explore in future work.

4.4 Inclination

The inclination of the observed galaxy must also have an effect on the asymmetry statistics. To explore this, Figs. 9-10 show the inclination dependence for the Shock Sim and Fly-by Sim respectively. In Fig. 9 the Shock-Sim is viewed at $\Theta = 0^\circ$, while in Fig. 10 the Fly-by Sim is viewed at $\Theta = 290^\circ$. The viewing angles are selected to have enough asymmetries in the profile at moderate inclinations that they can show the effect of inclination variation. Additionally, it is worth noting that the profiles have very high S/N ratios and the bin widths are 5 km s^{-1} . As such, the decrease in number of channels in near face-on galaxies will still be in the reliable regime according to Fig. 4.

The inclination dependence of the Shock Sim is quite in-

teresting. Both \mathcal{A} and $\mathcal{A}(v_{sys})$ are mostly constant along the range of inclinations, while the lopsidedness and ΔV generally increase as the system becomes more face-on. Once the galaxies become nearly face-on, all the asymmetry statistics go to zero. The collapse at this orientation is due to the profile reducing to a single-peaked Gaussian. Since the impact is edge-on, there are little, if any, systemic z velocities that project towards the observer.

In the Fly-By Sim, the vertical motions do cause changes in channel-by-channel statistics. Most interestingly, there is a peak in \mathcal{A} near $\sim 135^\circ$ and in $\mathcal{A}(v_{sys})$ at $\sim 150^\circ$. This is due to how the vertical perturbations of the galaxy project into the profile. These are also very local perturbations and give little to no lopsidedness.

The combination of Figs. 9-10 suggest that asymmetry measurements are relatively robust for inclinations greater than $15\text{-}20^\circ$. When galaxies are more face-on than this, the asymmetries decrease rapidly as the profiles become very

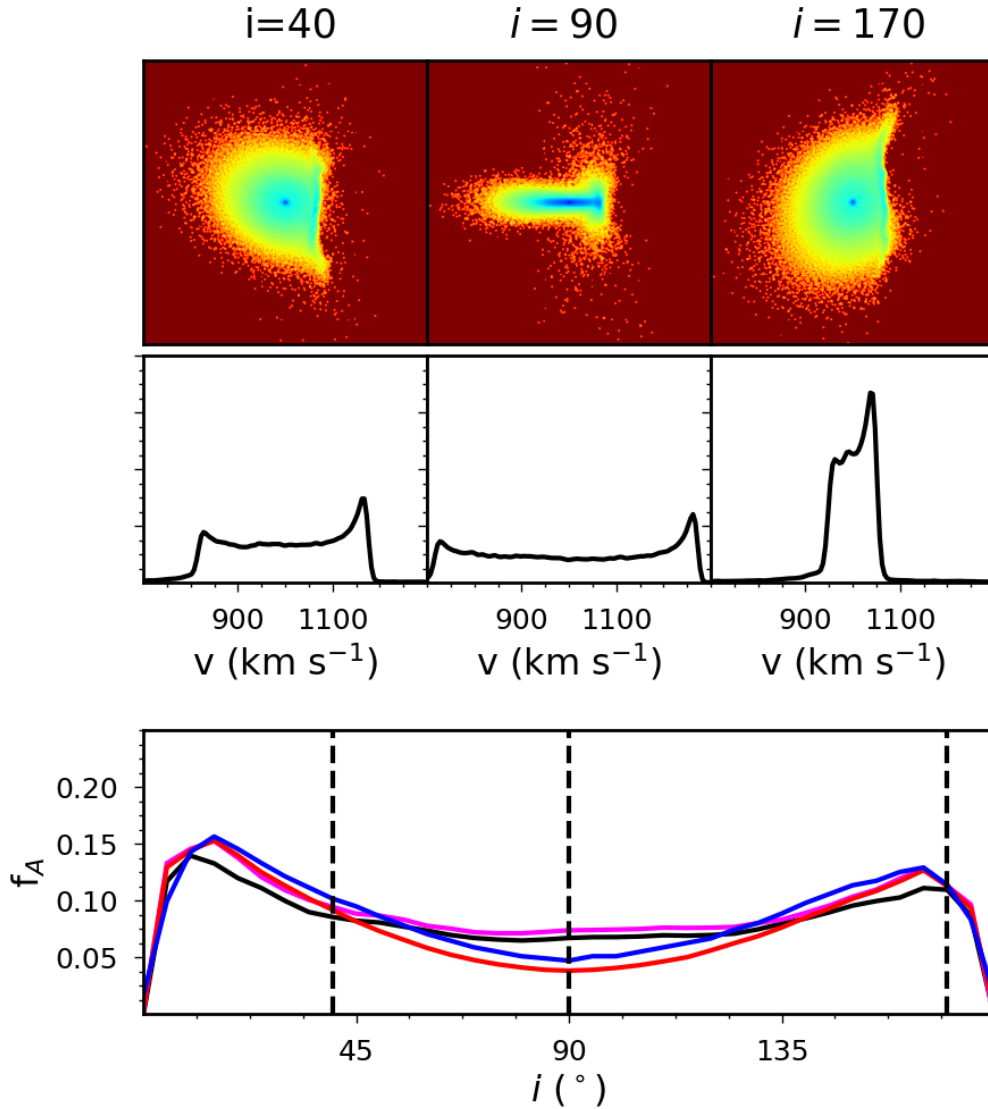


Figure 9. The asymmetry statistics for the Shock Sim as a function of inclination (bottom), along with a set of mock images (upper panels) and velocity profiles (middle panels) at specific inclinations. The lines are the same as in Fig. 7.

narrow. Related to this is the requirement of at least 10 resolution elements for even high S/N profiles (based on Fig. 4.)

5 THE WHISP SAMPLE

Moving from simulations, we have applied our statistics to a subsample of WHISP galaxies. The goal of this work is to explore how the various asymmetry statistics correlate with features of velocity profiles. To that end we also visually classified each profile using a variety of features (number of peaks, central dip depth, apparent asymmetry, etc.).

5.1 Data

We used observational data from WHISP (van der Hulst, van Albada & Sancisi 2001) to generate a subsample of velocity profiles for analysis. WHISP is an interferometric sur-

vey of 375 mostly late-type galaxies using the Westerbork Synthesis Radio Telescope and the data cubes, H I images, and velocity fields are publicly available². Three versions of the data cubes are available processed with different spatial resolutions. We chose to use the intermediate cubes with 30 arcsec \times 30 arcsec resolution so as to optimise the the signal-to-noise ratio per pixel while retaining good spatial resolution needed for two dimensional asymmetry analysis to be published in an upcoming paper, Hank et al. (2020). For most of the galaxies in the sample, the velocity resolution is 5 km s⁻¹.

Rather than using the full sample of WHISP galaxies, we have restricted ourselves to a subsample consisting of galaxies defined in Swaters et al. (2002) and Noordermeer et al. (2005). These galaxies have good S/N ratios, spatial and spectral resolution, and are sufficient for both the 1D

² <http://wow.astron.nl/>

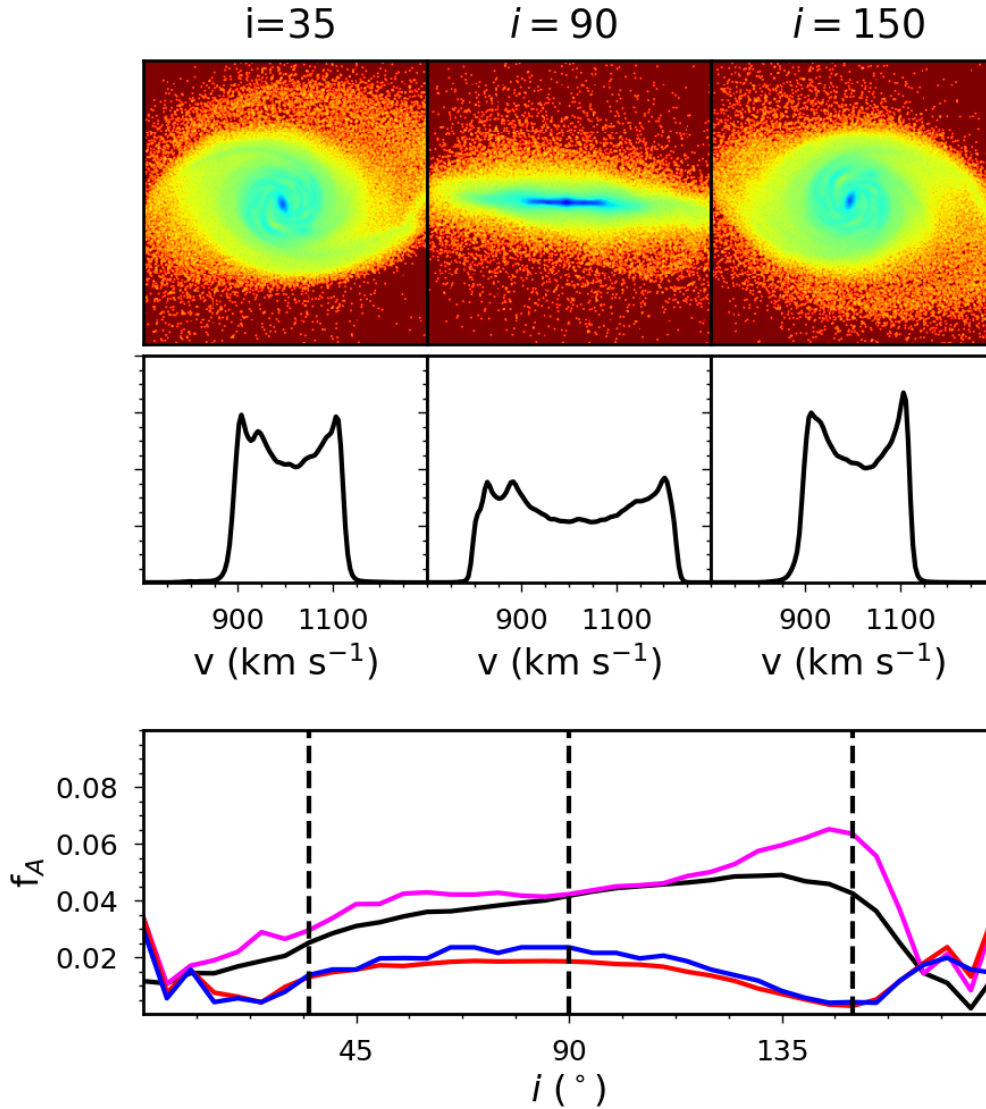


Figure 10. The asymmetry statistics for the Fly-by Sim as a function of inclination (bottom), along with a set of mock images (upper panels) and velocity profiles (middle panels) at specific inclinations. The lines are the same as in Fig. 7.

analysis performed here and the 2D work of Hank et al. (2020). They have also been well-studied in a variety of 2D morphological studies, including Holwerda et al. (2011) and Giese et al. (2016). Since we did not have the original mask cubes, we extracted the velocity profiles by using the H I image of each galaxy as a mask. We removed negative pixels, assuming they were due to noise, by calculating the RMS of only negative pixels in the image and then performing a 1σ cut on the full image before applying it as a mask. We applied the same mask region to each channel of the cube for each galaxy respectively and summed the total flux density in each channel to create a spectrum. As a result of not optimising the mask for each channel individually, the extracted profiles typically consisted of H I signal on a background pedestal. We estimated the pedestal by fitting a straight line between the average flux density values to the left and right away from the H I line and subtracted it from the spectrum to extract the final H I line profile. Some of

the profiles did not include enough channels to properly do a pedestal subtraction, leaving us with a final sample of 116 galaxies. The average peak S/N of these profiles is ~ 30 and all galaxies have sufficient channels for reliable asymmetry calculations.

5.2 By Eye Classification

Each velocity profile is both analyzed using the asymmetry statistics and classified by eye. The purpose of the by-eye classification is to see how well \mathcal{A} , A_L , or ΔV correlate with our judgement of the level of asymmetry in a global H I profile. Moreover, by classifying the galaxies, we can look for any clustering in parameter space and determine if there are any correlations.

Our visual classification scheme is quite basic. Firstly, we decide if a profile has a single or double peak. We then determine whether the profile is symmetric, slightly asymmet-

ric, moderately asymmetric, or very asymmetric. We examine whether the central region of the profile dips below 50% of the peak flux. This can only be true for double-peaked profiles. Finally, we classify the relative peak widths. This classification is the most complicated as there are three categories. The profile may have two peaks of differing widths, a single peak that is ‘diagonal’ (having strongly differing slopes leading to the peak), or the two peaks/one peak are the same width/symmetric respectively.

Three of the authors classified the galaxies first individually. Then, in cases where at least one person determined different levels of asymmetry, the three classifiers re-examined and re-classified those profiles together to obtain a consensus classification for all galaxies.

5.3 WHISP Asymmetries

Figure 11 shows the correlations between the three asymmetry statistics for our sample of 116 galaxies. There are a number of things to note in this plot. Firstly it is clear that A_L and ΔV are strongly correlated. This agrees with the results from the viewing angle and inclination studies. Given that ΔV is strongly related to the lopsidedness, this result is perhaps not too surprising.

There is a much weaker correlation of either channel-by-channel asymmetry measurement with the lopsidedness or ΔV . This is not surprising as \mathcal{A} is more sensitive to local asymmetries than either of the other statistics. There is a correlation between \mathcal{A} and $\mathcal{A}(v_{sys})$, where \mathcal{A} is, by design, always smaller. Nonetheless, this linear plot makes it somewhat difficult to investigate what is occurring at lower asymmetry levels.

It is also worth noting that the error bars on \mathcal{A} are generally smaller than those on A_L , ΔV , or even $\mathcal{A}(v_{sys})$. This is due to the fact that the asymmetry statistic is measured at v_{sym} and does not depend on v_{sys} . Therefore errors in the calculation of v_{sys} due to noise will not propagate into \mathcal{A} .

In order to examine some of the correlations and possible dependencies in greater detail, Fig. 12 shows the A_L - ΔV correlations on a log-log scale. In general, all the WHISP galaxies lie along the 1-1 line. This is unsurprising given that ΔV is related to A_L by v_{equal} .

There are a few relations that become clear in this figure. Firstly, and perhaps most importantly, the visual asymmetry classification spans the parameter space of both A_L and ΔV . There are galaxies classified as asymmetric with fairly low values of A_L and ΔV . This is due to the fact that the ‘by-eye’ classification accounts for both local and global features.

Secondly, there are a number of offsets that appear in different panels in Fig. 12. For instance, the irregulars are generally separated from the spirals in the middle panel. A clearer separation appears between the single and double peaked profiles. The cause of this separation, as well as the ‘equal peak width’ separation is ultimately due to the trends seen in the ‘central-dip’ panel.

To understand the central dip relationships Fig. 13 shows three profiles with similar values of A_L . This figure shows that, for given values of A_L , ΔV tends to be higher when the central dip is deeper (see the horizontal difference between the red and black vertical dashed lines in Fig. 13).

This is due to the nature of the ΔV statistic itself. As v_{fold} moves away from v_{sys} it moves flux from one of the integrals to the other. This increases/decreases L and inversely affects H . If v_{sys} is located near a peak, shifts in v_{fold} will move proportionally more flux than cases where v_{sys} is located near the central dip. As such, profiles with deeper dips will need to move v_{fold} further away to get equivalent shifts of flux from L to H . Therefore, for a given value of A_L , ΔV will be larger when the central dip is deeper.

This result also explains why profiles with greater widths generally lie above the one-to-one line. Wider profiles are more often double-peaked with deeper dips. Inversely, inclination can shrink profiles with deep dips, and, in the limit of face-on, transform them to single peaked profiles. Therefore the narrow profiles will have fewer deep central dips and lie lower on the $A_L - \Delta V$ trend.

In this figure there is no clear dependence on inclination. However there is a hint of a trend in the S/N, with higher S/N objects having larger ΔV values. It is also worth noting that the WHISP sample is selected to have both high peak S/N values, thus there are few objects below a S/N cut of 10.

Moving from the $A_L - \Delta V$ correlations, Fig. 14 shows the difference between the signal asymmetry, \mathcal{C} and the measured asymmetry, \mathcal{A} , and how they correlate with A_L . When calculated at v_{sys} , \mathcal{C} is always larger than A_L . This naturally flows from the definitions of Eq. 4 and Eq. 9. When \mathcal{C} is calculated at the ‘velocity of symmetry’, \mathcal{C} decreases. One of the effects of this decrease is to help to separate the profiles by their visual classification. However, the greatest separation of the profiles by visual classification is in \mathcal{A} calculated at v_{sym} . In that panel, it is clear that the asymmetry statistic, calculated at the ‘velocity of symmetry’, with the background subtraction, is the most correlated with our visual asymmetry classification.

To help make this point more clear, Fig. 15 shows histograms of these 5 statistics for each of the visual classifications. The large overlap in histograms for A_L indicates that the visual classifications are not strongly correlated with lopsidedness. \mathcal{C} is reasonably separated, but, since there is no background subtraction, the symmetric, slightly asymmetric, and moderately asymmetric still have large amounts of overlap. The greatest separation of the different histograms is for \mathcal{A} . This indicates that the full channel-by-channel asymmetry, measured at the ‘velocity of symmetry’, is the asymmetry statistic that correlates best with visual asymmetry classifications.

Figure 16 focuses on the \mathcal{A} - A_L correlation and its relation to other parameters. This plot shows a number of features. Firstly, profiles with a larger width tend to have larger values of \mathcal{A} . This result points to a profile resolution effect. However, this is not completely clear as WHISP profiles have velocity resolutions of 2, 4, 8, or 16 km s⁻¹ depending on their global profile width. For this reason we’ve added the number of elements in the upper middle panel of Fig. 16. That panel shows more clearly that profiles with more channels tend to have higher values of \mathcal{A} for a given value of A_L . This is consistent with Fig. 4, which shows that when the number of channels in a profile is below some limit (generally 20), \mathcal{A} tends to decrease while the uncertainties increase. The \mathcal{A} -profile width result seen in Fig. 16 is possibly a the manifestation of this trend. It points to the need to be careful in

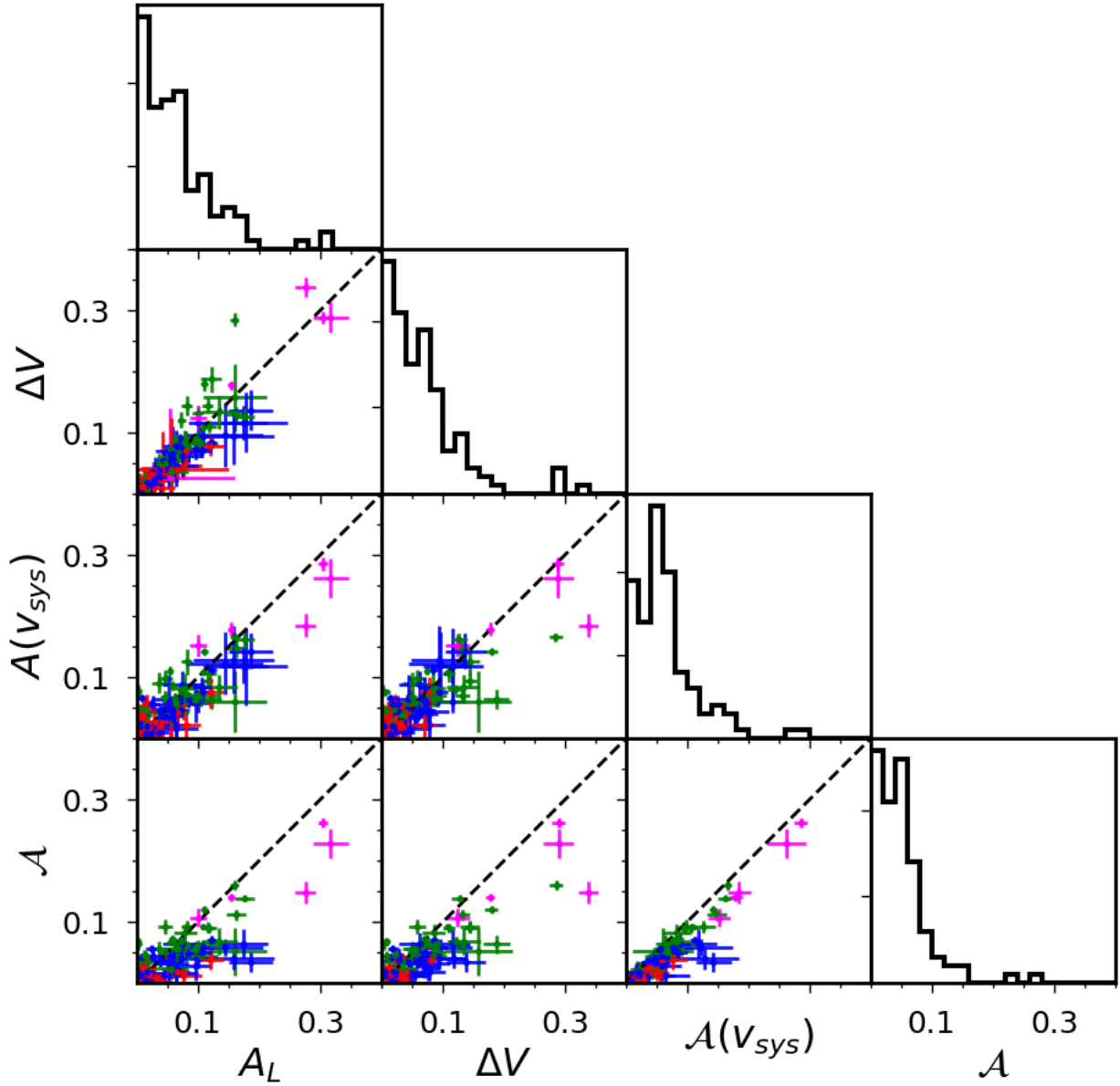


Figure 11. The WHISP galaxy asymmetry statistics. The red, blue, green, and magenta points are profiles classified as symmetric, slightly asymmetric, moderately asymmetric, and very asymmetric by eye. The dashed black lines in the correlation plots shows the 1-1 line. The histograms show the distribution of each statistic for the full sample. The error bars were determined by creating 100 mock profiles with Gaussian noise added to them based on the measured S/N . The one sigma error bars calculated from that sample are shown in the correlation plots.

both interpreting \mathcal{A} distributions and comparisons between specific profiles.

The trend with profile width also explains the trends seen in the galaxy-type, number of peaks, and central dip panels of Fig. 16. The spiral galaxies tend to have larger widths than the irregulars. It is also less likely to get double-peaked profiles with narrow widths. And, as discussed for the

profile width trends seen in Fig. 12, narrow profiles tend to have shallower central dips.

The ‘Equal Peak Width’ panel in Fig. 16 shows that double peaked profiles with different peak widths tend to have the largest values of \mathcal{A} , while they are spread across all values of A_L . This result is due to the fact that A_L calculates the global flux ratios while \mathcal{A} is sensitive to how the flux is distributed on a channel-by-channel basis. This same trend

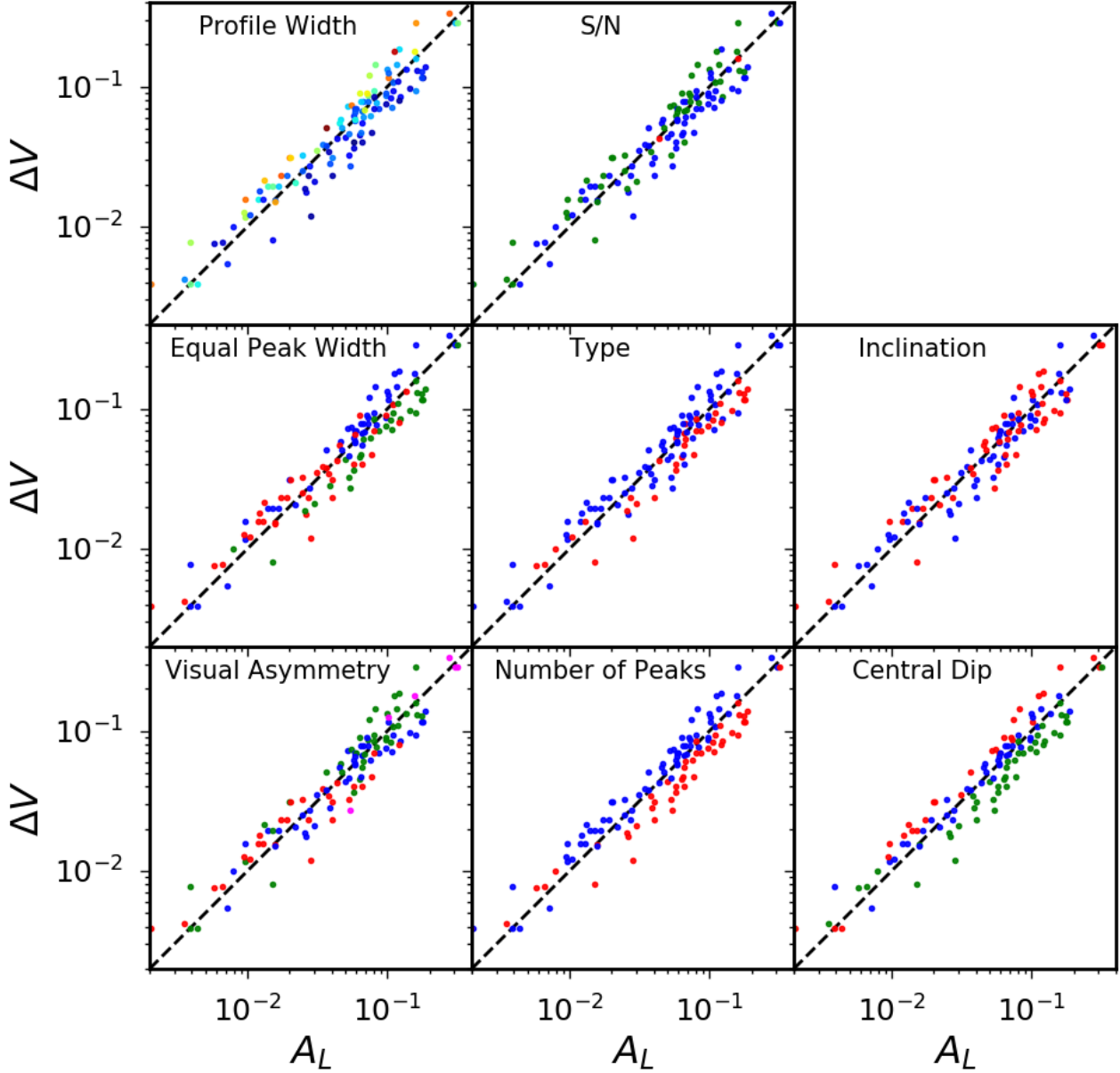


Figure 12. Lopsidedness- ΔV correlations. The bottom-left panel uses the same colors as Fig. 11. In the bottom-middle panel the red and blue points have one or two peaks. In the bottom-right panel the green, blue, and red points have a single peak, a central dip that is above the 50% flux level, and a central dip below the 50% level respectively. In the middle-left panel the green, blue, and red points have single peaks with differing slopes, two peaks with differing widths, or have symmetrical peak widths/single peaks that have similar slopes. In the middle panel, the red and blue points are irregular or spiral galaxies. The middle right panel has galaxies with $30^\circ \leq i \leq 60^\circ$ in blue and the other inclinations in red. The upper-left panel has a continuum of colors where dark blue points have small profile widths and cyan-red points have larger profile widths, with red as the largest. Finally, the upper-middle panel has objects with $S/N < 10$ in red, those with $10 \leq S/N < 30$ in blue and those with $S/N \geq 30$ in green.

is seen, but on a weaker level, for single peaks with differing slopes.

As with Fig. 12, there is no clear trend with inclination. There is a clear trend with S/N, where galaxies that have higher S/N values tend to have larger \mathcal{A} for the same A_L .

This trend can be understood from the results of Fig. 3. There A_L rapidly decreases to an asymptotic value, but, due to the background subtraction, \mathcal{A} has a slow increase with S/N. As such, it is unsurprising that real galaxies with less noise tend to have larger values for \mathcal{A} . It is perhaps best to

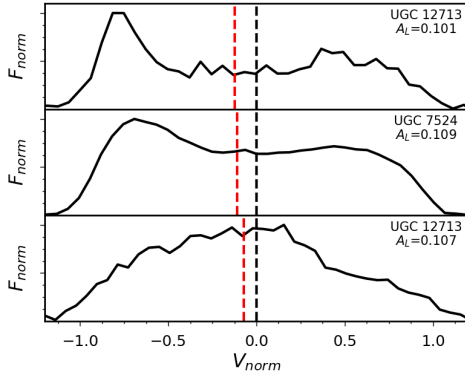


Figure 13. Three sample profiles with similar values of A_L . The y-axis is the flux normalized by the peak flux of each profile, while the x-axis shows the velocity shifted by v_{sys} and normalized by the width of each profile. The solid black line shows the profile, while the vertical dashed black and red lines show v_{sys} and the value of v_{fold} where the integrated flux on either side of the red line is equal.

think of \mathcal{A} as a minimum due to the amount of asymmetry in the signal region that may be attributed to the background.

Finally, this figure also shows the same result as Fig. 15; namely that \mathcal{A} correlates better with the by-eye classification than A_L . Generally, the profiles classified as moderately or strongly asymmetric have larger values of \mathcal{A} than the slightly asymmetric or symmetric profiles. Conversely, there are slightly asymmetric profiles with fairly large values for A_L and moderately asymmetric profiles with quite low A_L values. In other words, \mathcal{A} better represents what we perceive to be asymmetric. However, it is important to note that both \mathcal{A} and our visual classification are biased towards wider profiles. This is due to wider profiles having more channels and are therefore able to show more locally asymmetric features.

6 CONCLUSIONS

In this work we have developed two new general statistics to quantify the asymmetry of a velocity profile; \mathcal{A} and ΔV . Of these, \mathcal{A} can be calculated at both the systemic velocity and the ‘velocity of symmetry’. We have compared all three of these to the more commonly used lopsidedness statistic, A_L .

Using test profiles generated from the sum of Gaussian profiles, we explored how all the asymmetry statistics depend on v_{fold} and S/N . The lopsidedness statistic is defined in such a way that it always has a minimum value of zero. Conversely \mathcal{A} , has a unique minimal value which depends on the profile. This minimum is located at v_{sym} , which is not necessarily equal to v_{sys} . From these results we conclude that A_L should always be calculated at v_{sys} . The channel-by-channel asymmetry may be calculated at either v_{sys} or v_{sym} .

Lopsidedness and ΔV decrease to some asymptotic value as the S/N increases. The asymmetry statistic has the opposite behaviour due to the subtraction of a background

term. All the statistics rely on both sufficient S/N and resolution elements. In general, at low S/N , ~ 20 channels is necessary for a reliable asymmetry calculation. However, at higher S/N ratios, accurate measurements can be made with even 10 – 15 elements.

We also explored the dependence of the three statistics on viewing angle and inclination using two snapshots from simulations of interacting galaxies. The fact that a velocity profile is a combination of the projection of kinematic and morphological asymmetries along a particular line of sight means that profiles depend strongly on the viewing angle. As such, the four statistics vary significantly as the viewing angle changes. However, \mathcal{A} is the most stable against viewing angle variations. In both snapshots, for certain viewing angles, $A_L = \Delta V = 0$, even through the underlying gas dispersion is objectively asymmetric. Nonetheless, the viewing angle result points to the difficulty in interpreting asymmetry statistics for a single profile. While an asymmetric profile almost certainly indicates that the galaxy is disturbed, a symmetric profile does not necessarily indicate an undisturbed galaxy. So it is possible to make conclusions about *individual* asymmetric galaxies, it is not possible to do so for symmetric galaxies. But, it is possible to apply the statistics to large samples and make conclusions about *populations* of symmetric and asymmetric galaxies.

Similarly, \mathcal{A} is also slightly more stable against inclination. While A and ΔV vary significantly in the Shock Sim, \mathcal{A} is constant for most inclinations. It is worth noting that any dependence on inclination in this test is also degenerate with a dependence on resolution. As the vertical motions are relatively small, the dominant effect of changing the inclination is to change the number of bins spanning the profile. In the Fly-by Sim, the vertical motions lead to significant effects on \mathcal{A} and $\mathcal{A}(v_{sys})$ with peaks occurring as the profile becomes more face-on. Based on our results we would suggest only applying these statistics to galaxies with inclinations above $15 - 20^\circ$.

Finally, we applied all three statistics to a subsample of real profiles drawn from WHISP. We first visually classified each profile according to their number of peaks, apparent asymmetry, central dip, and the shape of the peaks. We found that A_L and ΔV are strongly correlated. We also found that for a given value of A_L , profiles with deeper central dips have larger values of ΔV . This means that the $A_L - \Delta V$ space can be used to objectively select profiles with or without deep central dips, which also points to the possibility of using a combination of asymmetry parameters as a classification and selection tool for large upcoming surveys. However, it will be necessary to determine how the features identified by such a classification relate to the actual galaxy.

We also found \mathcal{A} is more strongly correlated with the visual classification than either of the other statistics. In other words, the channel-by-channel asymmetry statistic calculated at the ‘velocity of symmetry’ is a superior indicator of non-axisymmetric features in velocity profiles than the lopsidedness or ΔV statistics.

The purpose of this paper was to introduce two new methods of characterizing velocity profiles. These methods, combined with the lopsidedness are promising new tools for upcoming surveys. The asymmetry statistics are sensitive to profile features not captured in the v_{sys} , profile width,

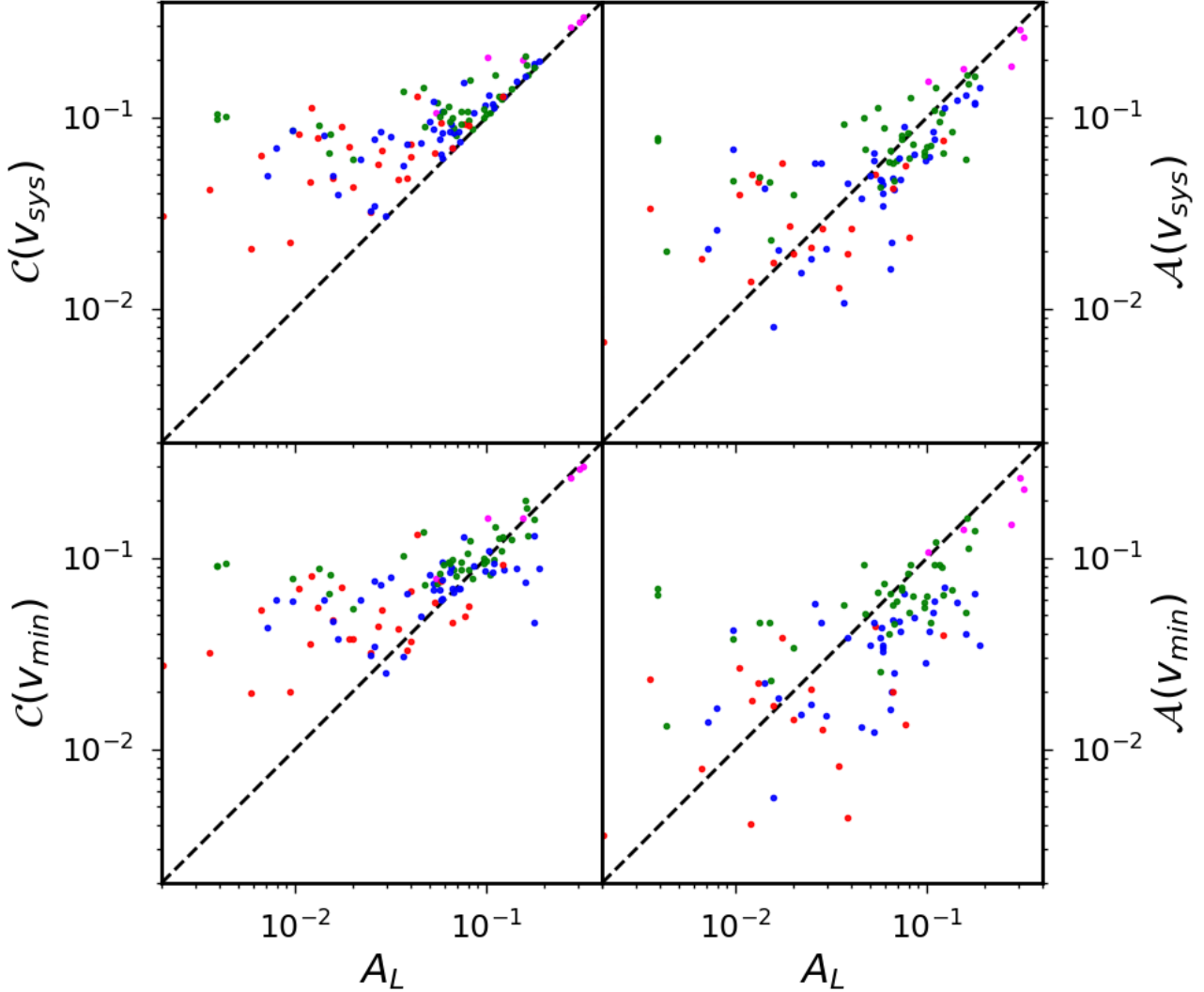


Figure 14. Detailed Asymmetry-Lopsidedness correlations. The point colors represent our visual classification for each galaxy and match the colors in Fig. 11. The upper-left panel shows the correlation between C calculated at v_{sys} and A_L while the lower-left panel shows C calculated at v_{sym} . The upper-right and lower right panels show A calculated at v_{sys} and v_{sym} respectively.

and integrated flux. Such features may arise from a variety of effects, like environment, merger histories, the method of gas accretion, etc.

The variation of the different statistics on viewing angle suggests that the measured values are not necessarily reliable for a single galaxy. However, when they are applied to a sample they can give information about the populations. This is partially seen in our work on the WHISP sample.

Our approach has been to develop profile characterization methods first and to understand how they depend on

a variety of unavoidable observational effects. The intention behind these new asymmetry definitions is to use them to identify the physical state/processes of a galaxy or population of galaxies (with the caveat that symmetric profiles do not always indicate undisturbed galaxies). But, in order to make conclusions about an object or population of objects it is necessary to understand the contributions from observational effects like S/N, resolution, inclination and viewing angle. This is what we accomplished in Secs. 3 and 4. In the future we will explore the relationship between these profile

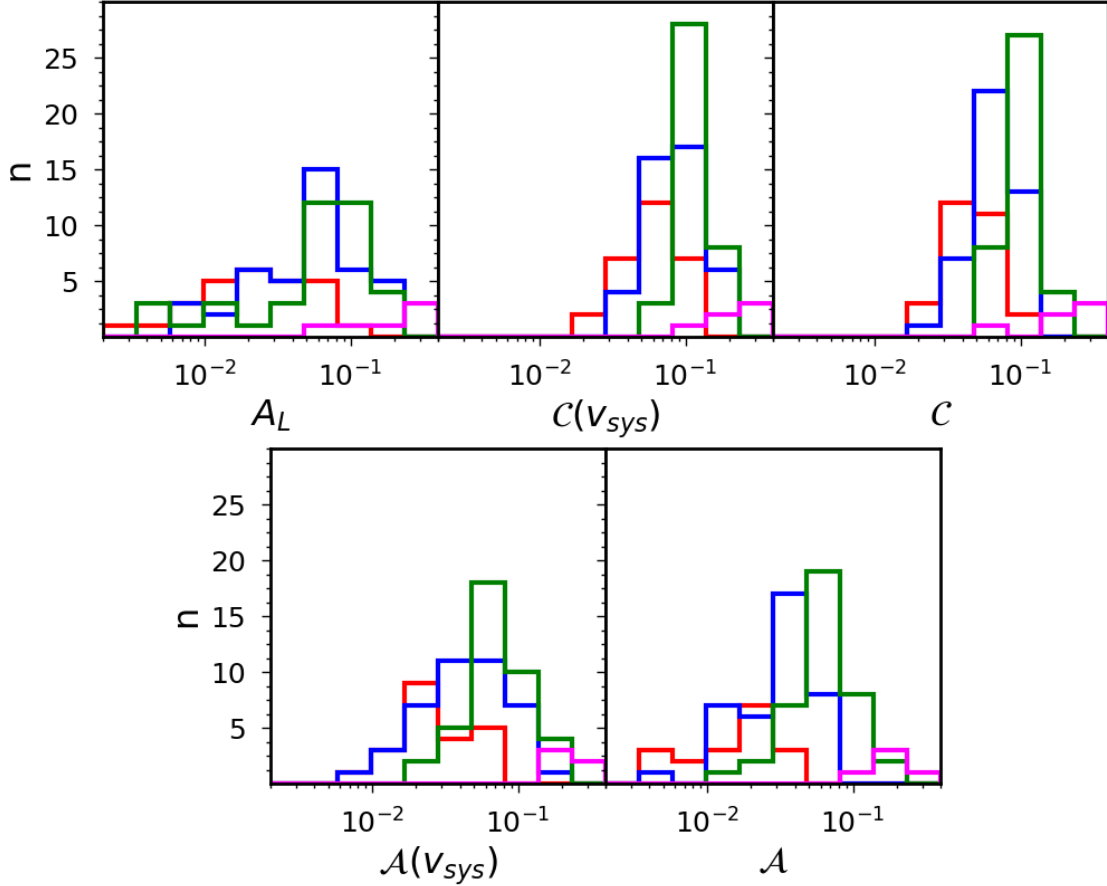


Figure 15. Histograms of the different asymmetry statistics depending on the visual classification. In each panel the red, blue, green and magenta lines represent profiles that are visually classified as symmetric, slightly asymmetric, moderately asymmetric, and very asymmetric (as in Fig. 11). The upper-left panel shows the lopsidedness, the upper-middle panel shows C calculated at v_{sys} and the upper-right panel shows C calculated at v_{sym} . The lower-left and lower-right panels show A calculated at v_{sys} and v_{sym} respectively.

statistics and 2D morphological statistics. We will also explore how they vary as a function of wavelength, and what correlations they have with the galaxy properties themselves (environment, star formation, etc.). Nonetheless, it is clear from Sec. 5 that profile asymmetry statistics do provide a useful method of characterizing galaxies and should be used to help analyze the sea of data produced by upcoming deep HI surveys like LADUMA and DINGO.

ACKNOWLEDGEMENTS

The authors wish to thank J. Bok for useful suggestions and inspiration. They would like to thank L. Cortese, A. Watts, L. Verdes-Montenegro, and K. Spekkens for their discussions. They would also like to thank T. Jarret, A. Comrie, A. Sivitelli, and the IDIA data visualisation lab for allowing

us to view the simulations in VR. We also wish to thank the referee for excellent suggestions for improving this paper. ND's work is supported by a SARCHI South African SKA Fellowship. NH acknowledges the bursary provided by South African Radio Astronomy Observatory. SK acknowledges the bursary provided by the NRF via the National Astrophysics and Space Sciences Programme. The numerical simulations were performed at the Centre for High Performance Computing.

REFERENCES

- Angiras, R. A., Jog, C. J., Omar, A., Dwarakanath, K. S., 2006, MNRAS, 369, 1849
 Abazajian K. N., et al., 2009, ApJS, 182, 543
 Arp, H., 1966, AJ Suppl. 14, 1.

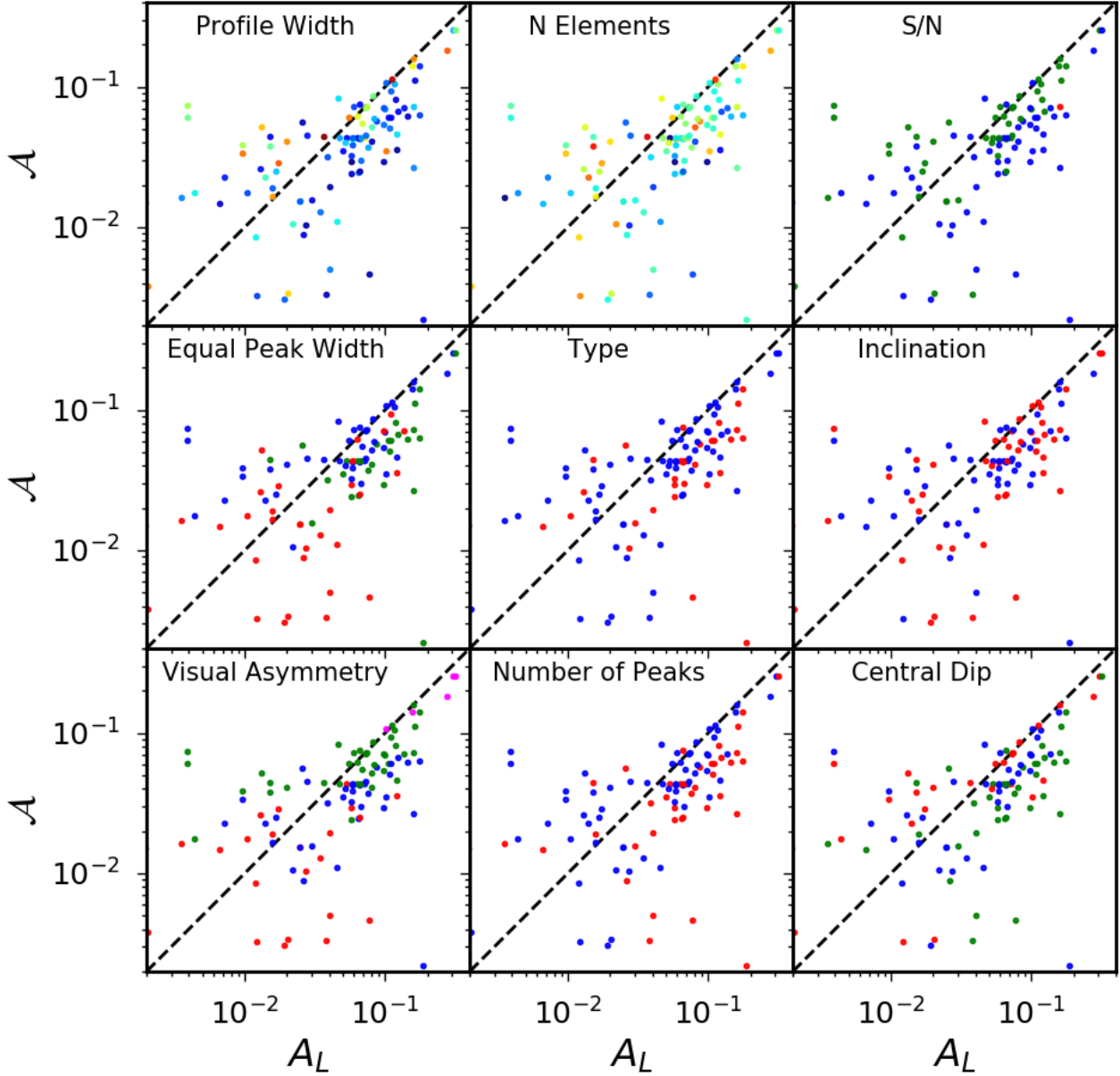


Figure 16. Lopsidedness-Asymmetry correlations. Panels and point colors are the same as Fig. 12 except that the S/N panel is now in the upper right. The upper middle panel shows the points colored by the number of channel elements within the profile where few to many channels goes from blue to red in the same manner as the profile width panel.

Bloom J. V., et al., 2017, MNRAS, 465, 123
 Bloom J. V., et al., 2018, MNRAS, 476, 2339
 Blyth S., et al., 2016, mks.conf, 4, mks.conf
 Bok J., Blyth S.-L., Gilbank D. G., Elson E. C., 2019, MNRAS, 484, 582
 Bournaud, F., Combes, F., Jog, C. J., Puerari, I., 2005, A&A, 438, 507
 Catinella, B., et al. 2018, MNRAS, 476, 875
 Catinella, B., et al. 2010, MNRAS, 403, 638
 Conselice, C. J., 2003, ApJS, 147, 1
 Conselice, C. J., Bershad, M. A., Jangren, A., 2000, ApJ, 529,

886
 Deg, N., Widrow, L., Randriamampandry, T., Carignan, C., 2019, MNRAS, 486, 5391
 Duffy A. R., et al., 2012, MNRAS, 426, 3385
 Espada D., Verdes-Montenegro L., Huchtmeier W. K., Sulentic J., Verley S., Leon S., Sabater J., 2011, A&A, 532, A117
 Fernández Lorenzo, M., Sulentic, J., Verdes-Montenegro, L., Argudo-Fernández, M., 2013, MNRAS, 434, 325
 Giese N., van der Hulst T., Serra P., Oosterloo T., 2016, MNRAS, 461, 1656
 Gunn, J. E., Gott, J. R. III, 1972, ApJ, 176, 1

- Hank, N., Blyth, S., Deg, N. 2020, in prep
- Haynes, M. P., Hogg, D. E., Maddalena, R. J., Roberts, M. S., van Zee, L., 1998, AJ, 115, 62
- Haynes, M. P., Giovanelli, R., Kent, B. R., et al. 2018, ApJ, 861, 49
- Holwerda B.W., Pirkal N., de Blok W. J. G., Bouchard A., Blyth S.-L., van der Heyden K. J., 2011, MNRAS, 416, 2437
- Jarvis M., et al., 2016, mks..conf, 6, mks..conf
- Kereš, D., Katz, N. Weinberg, D. H., Davé, R., 2002, MNRAS, 363, 2
- Kornreich D. A., Haynes M. P., Lovelace R. V. E., van Zee L., 2000, AJ, 120, 139
- Lelli, F., Verheijen, M., Fraternali, F., 2014, MNRAS, 445, 1694
- Lotz J. M., Primack J., Madau P., 2004, AJ, 128, 163
- Matthews L. D., van Driel W., Gallagher III J. S., 1998, AJ, 116, 1169
- Meyer, M. J., Zwaan, M. A., Webster, R. L., Staveley-Smith, L., et al., 2004, MNRAS, 350, 1195
- Mundy, C., J., Conelice, C., J., Duncan, K., J., Almaini, O. Häußler, B. Hartley, W., G., 2017, MNRAS, 470, 3507
- Newville, M., Stensitzki, T., Allen, D. B., Ingargiola, A., 2014, LMFIT: Non-Linear Least-Square Minimization and Curve-Fitting for Python, Zenodo, doi:10.5281/zenodo.11813
- Noordermeer, E., van der Hulst, J. M., Sancisi, R., Swaters, R. A., van Albada, T. S., 2005, A&A, 442, 137
- Peterson, S. D., Shostak, G. S., 1974, AJ, 79, 767
- Reichard, T. A., Heckman, T. M., Rudnick, G., Brinchmann, J., Kauffmann, G., 2008, ApJ, 677, 186
- Richter, O.-G., Sancisi, R., 1994, A&A, 290, L9
- Sancisi R., Fraternali F., Oosterloo T., van der Hulst T., 2008, A&ARv, 15, 189
- Schade, D., Lilly, S. J., Crampton, D., Hammer, F., Le Fevre, O., Tresse, L., 1995, ApJ, 451, L1
- Shapiro K. L., et al., 2008, ApJ, 682, 231
- Springel, V., 2005, MNRAS, 464, 1105
- Stewart I. M., Blyth S.-L., de Blok W. J. G., 2014, A&A, 567, A61
- Swaters, R. A., van Albada, T. S., van der Hulst, J. M., Sancisi, R., 2002, A&A, 390, 829
- Tift W. G., Cocke W. J., 1988, ApJS, 67, 1
- Trujillo I., Aguerrri J. A. L., Cepa J., Gutiérrez C. M., 2001, MNRAS, 328, 977
- van der Hulst J. M., van Albada T. S., Sancisi R., 2001, ASPC, 451, ASPC..240
- van Eymeren, J., Jütte, E., Jog, C. J., Stein, Y., Dettmar, R. -J., 2011, A&A, 530, A29
- Watts A. B., Catinella B., Cortese L., Power C., 2020, MNRAS, 492, 3672
- Westmeier T., Jurek R., Obreschkow D., Koribalski B. S., Staveley-Smith L., 2014, MNRAS, 438, 1176
- Wisnioski, E., et al. 2019, ApJ, 886, 124
- Wilcots E. M., Prescott M. K. M., 2004, AJ, 127, 1900

This paper has been typeset from a $\text{\TeX}/\text{\LaTeX}$ file prepared by the author.